THESIS

ESTIMATING THE LIKELIHOOD OF SIGNIFICANT CLIMATE CHANGE WITH THE NCAR 40-MEMBER ENSEMBLE

Submitted by

William Eliott Foust

Department of Atmospheric Science

In partial fulfillment of the requirements

For the Degree of Master of Science

Colorado State University

Fort Collins, Colorado

Fall 2014

Master's Committee:

Advisor: David Thompson

David Randall
Elizabeth Barnes
Daniel Cooley

ABSTRACT

ESTIMATING THE LIKELIHOOD OF SIGNIFICANT CLIMATE CHANGE WITH THE NCAR 40-MEMBER ENSEMBLE

Increasing greenhouse gas concentrations are changing the radiative forcing on the climate system, and this forcing will be the key driver of climate change over the 21st century. One of the most pressing questions associated with climate change is whether certain aspects of the climate system will change significantly. Climate ensembles are often used to estimate the probability of significant climate change, but they struggle to produce accurate estimates of significant climate change because they sometimes require more realizations than what is feasible to produce. Additionally, the ensemble mean suggests how the climate will respond to an external forcing, but since it filters out the variability, it cannot determine if the response is significant.

In this study, the NCAR CCSM 40-member ensemble and a lag-1 autoregressive model (AR1 model) are used to estimate the likelihood that climate trends will be significant. The AR1 model generates an analytic solution for what the distribution of trends should be if the NCAR model was run an infinite number of times. The analytical solution produced by the AR1 model is used to assess the significance of future climate trends.

The results of this study demonstrate that an AR1 model can aid in making a probabilistic forecast. Additionally, the results give insight into the certainty of the trends in the surface temperature field, precipitation field, and atmospheric circulation, the probability of climate

trends being significant, and whether the significance of climate trends is dependent on the internal variability or anthropogenic forcing.

ACKNOWLEDGEMENTS

First, I would like to thank my parents for their love, encouragement, and unwavering support as I pursued a graduate degree. I would like to thank my advisor Dr. David W.J. Thompson for his guidance and mentorship, which has helped me to establish myself as a scientist. I would also like to thank each of the members of my committee, Dr. David A. Randall, Dr. Elizabeth Barnes, and Dr. Daniel Cooley, for their help, critiques, and suggestions. I would like to thank my friends and members of the Thompson research group for their support, help, and general conversations that have made my experience in Colorado all the better. Finally, I would like to thank all of those involved with the NSF grant *Analysis of Large-Scale Extratropical Climate Variability and Change*, which has made this research possible.

TABLE OF CONTENTS

Chapter 1

Introduction

1.1 Overview

Increasing greenhouse gas concentrations are changing the radiative forcing on the climate system, and will continue to do so throughout the 21st century. This forcing, known as the anthropogenic forcing, will be the key driver of climate change over the 21st century. One of the most pressing questions associated with climate change is whether local and regional climate will undergo significant changes. In order to predict local and regional climate change, coupled climate models are used to simulate the future climate. However, the signal of climate change on local and regional spatial scales will be superposed onto a large amount of natural internal climate variability, or *climate noise*, which makes it difficult for climate models to project climate change on relatively small spatial scales [*Santer et al.,* 2011]. The natural internal variability makes it difficult to project climate change, because the internal variability creates random noise within the climate. Since the noise is random, it is highly unlikely that a climate model will be able to simulate all aspects of the future climate perfectly.

The bounds of the internal variability and the certainty of climate projections can be assessed by running multiple climate change simulations in which only the initial conditions are perturbed from one simulation to the next. The resulting ensemble produces a collection of possible climate simulations that differ from one another, and the magnitude of these differences are proportional to the amplitude of the internal variability. Larger ensembles capture more of the variability in climate trends, which allows for a more accurate assessment of the certainty of climate change projections. Thus, it is beneficial to create as many realizations as possible.

However, the challenge of creating a large amount of realizations is that each realization is computationally expensive. Therefore, the size of a climate ensemble is limited by the computational resources available.

In this study, we use the NCAR 40-member ensemble to assess the impact of the internal variability on future climate projections. Forty ensemble members are sometimes insufficient to estimate the bounds of the internal variability, so we use a statistical model to supplement the 40 members of the NCAR ensemble [*Knutti et al.,* 2010]. The statistical model creates artificial time series that are based on properties of the CCSM model. Together, the NCAR ensemble and statistical model will be used to create estimated probability density functions, so that we may see the spread in future climate change projections. The results of this study provide insight on:

1) The certainty of future climate change projections

2) The likelihood that future climate trends will be significant

1.2 Uncertainty

Uncertainty is a term that is used in several different contexts within the climate sciences. An example of a subjective use of the uncertainty is when a researcher uses his knowledge of a malfunctioning instrument, biases in a model, errors within a model, or general problems within a data set to convey his disbelief in the accuracy of a given parameter [*Morgan et al.*, 2009]. Uncertainty can be used quantitatively when it describes the probability or likelihood of an event occurring. An example is given in Table 1.1, where the IPCC mapped uncertainty to probabilities. Ultimately, uncertainty is a term that has multiple uses, but it is important to define it within the context of this study. For this study, the term uncertainty is associated with climate

change predictions. When referring to climate projections, uncertainty characterizes the amount of spread in an ensemble of climate simulations [*Tebaldi et al.*, 2005; *Masson and Knutti*, 2011].

The uncertainty associated with climate change projections can be partitioned into three contributing sources: the anthropogenic emissions, climate models, and the internal variability of the climate system [*Deser et al.*, 2012]. The uncertainty caused by anthropogenic greenhouse gas emissions is referred to as the scenario uncertainty. This particular type of uncertainty is strongly coupled with human development and the global economy. If humans aggressively reduce greenhouse emissions, there will be a relatively weak anthropogenic forcing in the future. However, rapid human development and minimal effort to reduce greenhouse gas emissions will lead to a stronger anthropogenic forcing in the future [*Hawkins and Sutton*, 2009]. Hence, the spread in climate projections is partially dependent on the diversity of greenhouse gas emission scenarios.

In addition to greenhouse gas concentrations, climate projections are also dependent on model physics. Given the same forcing and initial conditions, climate projections will vary from one model to the next, which makes climate trends less certain. The uncertainty from climate models is due to discrepancies in model resolution and parameterization schemes. Climate models must parameterize processes such as cloud microphysics, small-scale turbulence, and surface energy fluxes that are spatially smaller than a grid cell. Since the models' parameterization schemes differ from one another, their output varies from one another as well. In addition to model physics and parameterization, rounding error can contribute to a difference in output amongst climate models. This error occurs because the output of a climate model is dependent on the computer's precision. Since the computers cause the models round differently, the errors compound and create different results [*Bailey et al.*, 2012].

Another prominent contributor to the uncertainty associated with climate projections is the natural internal variability within the climate system. The natural variability of the climate system exists without the application of an external forcing and arises from non-linear internal dynamics. The natural variability is essentially long-term stochastic red noise [*Deser et al.*, 2010]. The *climate noise* is superimposed onto the anthropogenic signal, which makes the forced component of the trends less certain.

The three primary sources of uncertainty in the surface temperature field are partitioned and displayed in Figure 1.1 [Hawkin and Sutton 2009]. The left panel shows the three primary sources of uncertainty in the global mean surface temperature, while the right panel shows the uncertainty in the surface temperature field over the British Isles (the British Isles are used to represent an arbitrary regional spatial scale). The internal variability, model, and scenario uncertainty are shaded orange, blue, and green respectively. The fraction of total variance is the ratio of the variance due to one of the sources of uncertainty over the total variance.

The left panel of the figure indicates that climate models are the most dominant source of uncertainty for near-term climate change on a global spatial scale. The figure also reveals that the internal variability makes a substantial contribution to the uncertainty in the global mean surface temperature field on sub-decadal timescales. Contrarily, the scenario uncertainty is the most dominant source of uncertainty in long-term climate change.

The right panel suggests that the internal variability is the most dominant source of uncertainty in near-term regional climate. On regional scales, the amplitude of the internal variability is high, which causes climate projections to be less certain. Over decadal time scales, the solutions produced by climate models diverge, and cause the model uncertainty to become

more prominent. After roughly 50 years, the scenario uncertainty is the most dominant source of uncertainty on all spatial scales.

In order to make more reliable projections, the uncertainty must be reduced. The scenario uncertainty can be reduced by acquiring better estimates of population growth, developing better policy and economic models. The model uncertainty can be reduced by resolving or parameterizing fine scale processes. Unlike the other sources of uncertainty, the internal variability uncertainty cannot be reduced, since it is random and independent of anthropogenic influences. However, assessing the magnitude of the internal variability can help us to estimate how the natural variability will impact the future climate. This study will use a climate ensemble to measure the internal variability uncertainty and determine how it affects climate change projections.

1.3 Climate Models and Ensembles

A global climate model is a mathematical representation of the land surface, cryosphere, ocean, and atmosphere. Each component of the climate model simulates one aspect of the climate system, and the components are coupled together with equations to simulate the interactions within the climate system [*IPCC AR4,* 2007]. Since climate models are coupled, they account for the interactions, feedbacks, and other complexities that lie within the climate system and produce a more realistic and comprehensive representation of the climate.

A climate ensemble uses global climate models to produce a collection of unique climate simulations that span the same time domain. The different realizations of the ensemble produce a spectrum of possible outcomes, because the output from one model or realization is different from the next. Climate ensembles can be generated by running multiple models that are

independent from one another (perturbed physics ensemble), running a single model and changing the forcing (perturbed forcing ensemble), running a single model and changing the initial conditions (perturbed initial condition ensemble), or any combination of those listed above.

A perturbed physics ensemble assesses how model physics, parameterization schemes, and resolution impact climate change simulations. This type of ensemble relies on the premise that climate models produce different results based on their parameterization schemes and resolution [*Sanderson et al.*, 2007]. Hence, the members of a perturbed physics ensemble can be generated by changing the parameterization scheme or resolution of a single climate model. [*Hawkins and Sutton*, 2009].

A perturbed forcing ensemble is an ensemble of climate simulations that use different anthropogenic forcings or greenhouse gas emission scenarios. With each simulation, the anthropogenic forcing can be controlled by either prescribing the concentrations of greenhouse gases, or changing the greenhouse gas emissions and transport within the model [*Hawkins and Sutton*, 2010]. Usually, perturbed forcing ensembles generate a larger spread than the perturbed physics ensemble. This is because climate models are more sensitive to the anthropogenic forcing than the model physics [*Hawkins and Sutton*, 2009]. Figure 1.2 is an example of a perturbed forcing ensemble. The figure shows the global mean surface temperature response to different anthropogenic forcing scenarios.

Perturbed initial condition ensembles are used to evaluate the effects of natural variability on the climate. With this type of ensemble, the initial conditions are changed for each ensemble member, while every other aspect of the climate model remains fixed. The different initial conditions cause the solutions to diverge, and the resulting ensemble members are unique

relative to one another [*Lorenz*, 1963]. Since all other aspects of the model remain fixed, the output from each ensemble member varies about the ensemble mean.

In this study, the NCAR CCSM 40-member ensemble (perturbed initial condition ensemble) is used to evaluate the affects of the natural variability on the future climate. As mentioned before, 40 ensemble members may not be sufficient to represent the full range and spread of possible climate trends. Studies show that larger ensembles offer better estimates of the spread in climate variables, which helps to assess the uncertainty caused by the internal variability [*Tebaldi and Knutti,* 2007]. To address this limitation, statistical models will supplement the realizations produced by the 40-member ensemble. Details on this process will be discussed further in the text.

1.4 Significance

A significance test is a statistical tool that is often deployed in atmospheric science. It determines the probability that an outcome is not due to chance [*Spiegel and Stephens,* 1998]. In the context of this study, statistical significance will be used to determine if trends are significantly different from zero. The significance test used in this study is adapted from *Santer* et al. 2000, and details on the calculations used will be discussed in latter sections of the text. The null hypothesis is that there does not exist a trend, or that the magnitude of the trend is zero. If trends are statistically significant, then the null hypothesis is rejected, and there is a strong possibility that the existence of a trend is due to the anthropogenic forcing, and not by chance. If the null hypothesis is not rejected, then there does not exist enough evidence to conclusively state that the anthropogenic forcing is driving the trend. Ultimately, the significance tests that are

employed in this study will determine whether the projected climate trends are driven by an anthropogenic forcing or chance.

1.5 Variables Studied

1.5.1 Surface Temperature

The surface temperature is a state variable that is important for many aspects of the climate, and it is often used as an indicator of climate change. Studies show that changes in regional surface temperature can serve as a proxy for biological and agricultural processes such as changes in growing regions, agricultural production, land use changes, and the health of ecosystems [*Pielke et al.,* 1998]. Additionally, the global mean surface temperature can be used to measure the sensitivity of the climate [*Manabe and Stouffer,* 1980].

Long-term changes in the local and regional surface temperatures, due to anthropogenic forcing, can be very difficult to detect because they are frequently masked by large internal variability in the climate system. The primary natural sources of variability on a regional scale include the internal variability of the climate and El Niño Southern Oscillation (ENSO). In particular, ENSO generally shows a random forcing that projects onto the surface temperature field, whereas the anthropogenic forcing is more consistent [*Thompson et al.,* 2009].

Because the surface temperature field is important for detecting climate change, we will use it as a focus in this study. Previous studies have shown that the global mean surface temperature field should show a weak warming trend over the next 50 years, but it is likely that the warming trend will vary widely on local spatial scales [*Deser et al.,* 2012]. In this study, we attempt to estimate how likely trends in the surface temperature field will be significant, which will be an indicator of climate change.

1.5.2 Precipitation

Changes in the precipitation field are important because they indicate changes in the hydrological cycle. Unfortunately, it is difficult to predict how local precipitation will respond to increasing greenhouse gas concentrations. As per the Clausisus-Clapeyron equation, a warmer atmosphere allows for higher saturation vapor pressures [*Held and Soden*, 2000]. Estimates are that the global mean precipitation will change by 1-3% per degree of global mean warming [*Wentz et al.*, 2007]. This is because evapotranspiration is expected to change by 1-3% per degree of warming, and the global mean precipitation should balance the evaporation. Since the projected change in precipitation is small and the internal variability is large, it may be difficult to detect such a change.

On regional scales, the precipitation field is noisy, which makes it difficult to detect the anthropogenic signal in precipitation at a specific location. As a result, future projections of local and regional precipitation are uncertain. Even though changes in precipitation are uncertain, changes in precipitation on relatively large scales was shown to be robust across the CMIP3 climate models in a study by *Held and Soden* [2006]. The study revealed that the anthropogenic forcing causes the annual mean precipitation to increase in the high latitudes and parts of the deep tropics, and decrease in the subtropics. This pattern of precipitation is sometimes referred to as *the dry get drier and the wet get wetter*, and is shown in Figure 1.3. This pattern has merit, because the study used observations to show that precipitation trends have been following this pattern over the last 30 years.

In this study, we will assess how the internal variability can affect the large-scale precipitation response to anthropogenic forcing. We will observe the Northern and Southern

Hemisphere subtropics, as well as the deep tropics. If the internal variability is large, then it is possible that the internal variability can mask the anthropogenic signal, and prevent us from observing a drying of the subtropics and a moistening of the deep tropics.

1.5.3 Atmospheric Circulation

Some aspects of the atmospheric circulation may undergo significant changes in response to the anthropogenic forcing. It is important to know the extent of these changes, because the circulation has been shown to influence many state variables [*Thompson and Wallace*, 2000b; *Deser et al.*, 2014]. Although there are many measures and components of the atmospheric circulation, this study will limit the circulation to the annular modes, jet latitude, and width of the tropics.

1.5.3.1 Annular Modes

The Northern and Southern Hemisphere annular modes (NAM and SAM) are large hemispheric-scale patterns of variability in the climate system. They are characterized by dipoles in the pressure field between the middle and high latitudes. The positive [negative] phase of the annular modes is marked by anomalously low [high] pressure in the high latitudes and anomalously high [low] pressure in the mid latitudes. The e-folding time scale of the annular modes is roughly 10 days. The annular modes explain roughly 25-30% of the variability in the surface temperature field within their respective hemisphere (see Figure 1.4) [*Thompson and Wallace*, 2000a].

GCMs predict that the Northern Hemisphere and Southern Hemisphere annular modes will trend towards their positive phase in response to an anthropogenic forcing over the next 50

years [*Miller et al.*, 2006]. However, the exact mechanisms for this response is yet to be determined. Comparatively, GCMs suggest that the magnitude of future SAM trends will be weaker than the NAM trends [*Gillett and Fyfe,* 2013]. SAM trends are likely to be weaker, because ozone recovery in the Southern Hemisphere forces the SAM toward its negative phase, while increasing greenhouse gases force the SAM towards its positive phase. Hence, the SAM is currently undergoing a competition between greenhouse warming and ozone recovery. This competition is expected to continue until the ozone hole fully recovers (approximately 2050) [*Polvani et al.*, 2011]. After the ozone hole recovers, the SAM should continue to shift towards its positive phase.

It is important to assess the significance of the annular mode trends on interannual and decadal timescales, because they represent human-induced changes to the large-scale circulation. Additionally, the analysis performed in this study will help us to understand how much the internal variability influences the annular mode trends.

1.5.3.2 Jet Latitude

This study will assess the likelihood of significant changes to the eddy-driven jet. We analyze changes in the jet, because the latitudes of the jet streams are strongly correlated with the index of the annular modes [*Woollings and Blackburn,* 2012]. Hence, a positive NAM or SAM index corresponds to a poleward jet shift. Since these are viewed in tandem, the position of the jet serves as an indicator of how the circulation changes.

1.5.3.3 Hadley Cell and Width of the Tropics

The Hadley circulation is comprised of two thermally direct meridional overturning cells. Low-level convergence and upper-level divergence mark the rising branch of the Hadley cell, while dry and subsiding air marks the outward edges of the cells. The Hadley cell is important for this study, because the poleward edges in the Northern and Southern Hemisphere are used to define the width of the tropics, and the poleward extent of the Hadley circulation is shown to be coupled the annular modes and the position of the eddy-driven jet [*Previdi et al.,* 2007; *Kidston et al.,* 2013]. A schematic of the general circulation is shown in Figure 1.5. Took out a sentence

The Hadley cell is expected to expand poleward and weaken in response to climate change, but there exists a substantial amount of uncertainty in regards to the extent of this expansion. [*Frieson et al.,* 2007; *Lu et al.,* 2007; *Kang et al.,* 2013]. An expansion of the Hadley cell represents changes in the tropical circulation. If significant changes are detected in the Hadley cell, then it should be relatively easy to observe significant changes in other components of the atmospheric circulation.

Table 1.1 The IPCC definitions of certainty and uncertainty. Taken from the U.S. Climate Change Science Program Synthesis and Assessment Product.

Word	Probability range
Virtually certain	>0.99
Very likely	0.9-0.99
Likely	0.66-0.9
Medium likelihood	0.33-0.66
Unlikely	0.1-0.33
Very unlikely	0.01-0.1
Exceptionally unlikely	<0.01

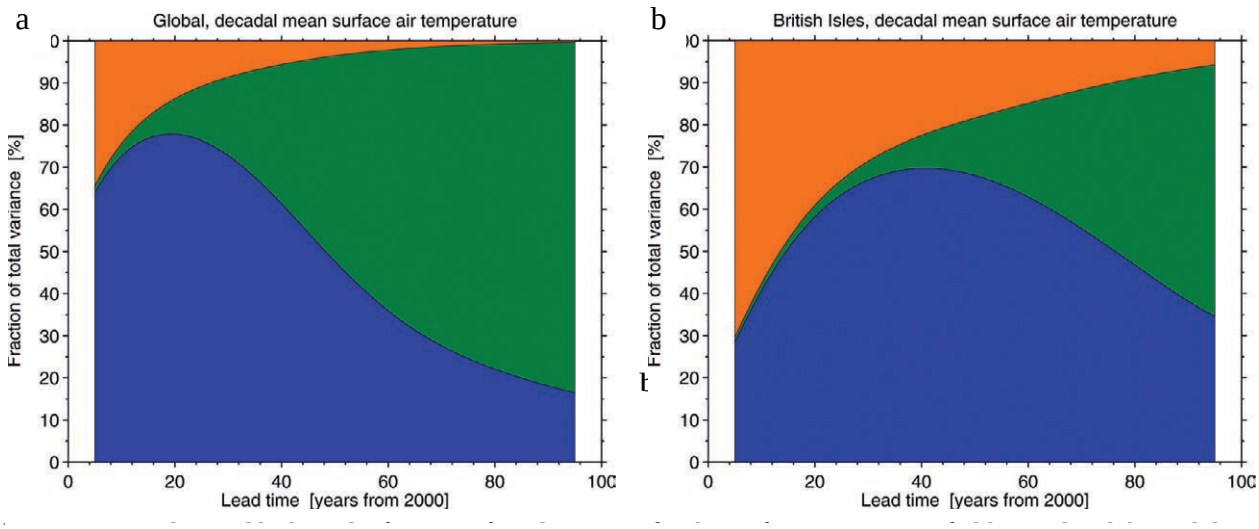

Figure 1.1 Panels a and b show the fraction of total variance for the surface temperature field over the globe and the British Isles respectively. The green regions represent the scenario uncertainty, the blue regions represent the model uncertainty, and the orange regions represent the internal variability uncertainty. This figure shows that the most dominant source of uncertainty on local scales are from the internal variability, while the greenhouse gases are the largest contributors to the uncertainty in the global mean temperature field. Figure taken from *Hawkin and Sutton, 2009.*

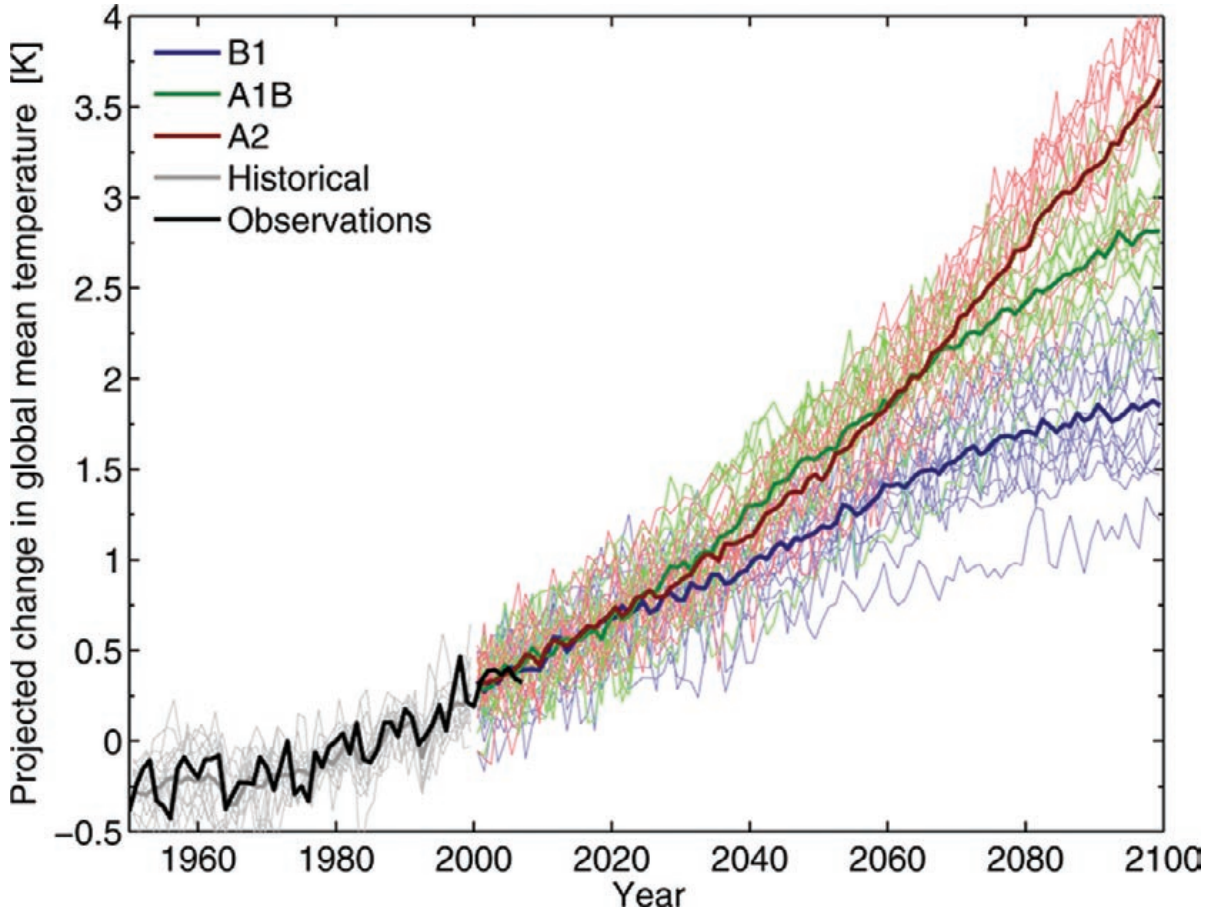

Figure 1.2 A total of 15 CMIP3 ensemble global mean surface temperature projections forced with the B1, A1B, and A2 forcing scenarios. The multi-model mean is represented by the thick solid lines. The gray lines represent the historical runs, and the black line represents the observations. Projections are from 2000-2100, and the observations are from 1950-2007. Anomalies are calculated with 1971-2000 mean. Figure taken from *Hawkin and Sutton, 2009.*

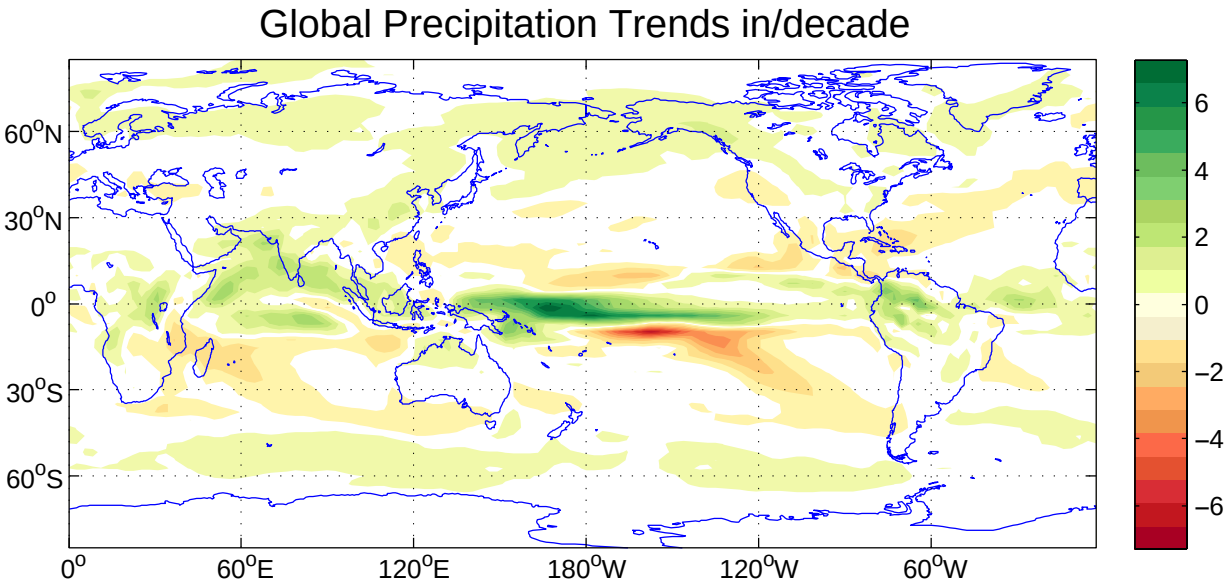

Figure 1.3 A map of the NCAR CCSM 40-member ensemble 2000-2060 ensemble mean precipitation trends. Units are inches/decade

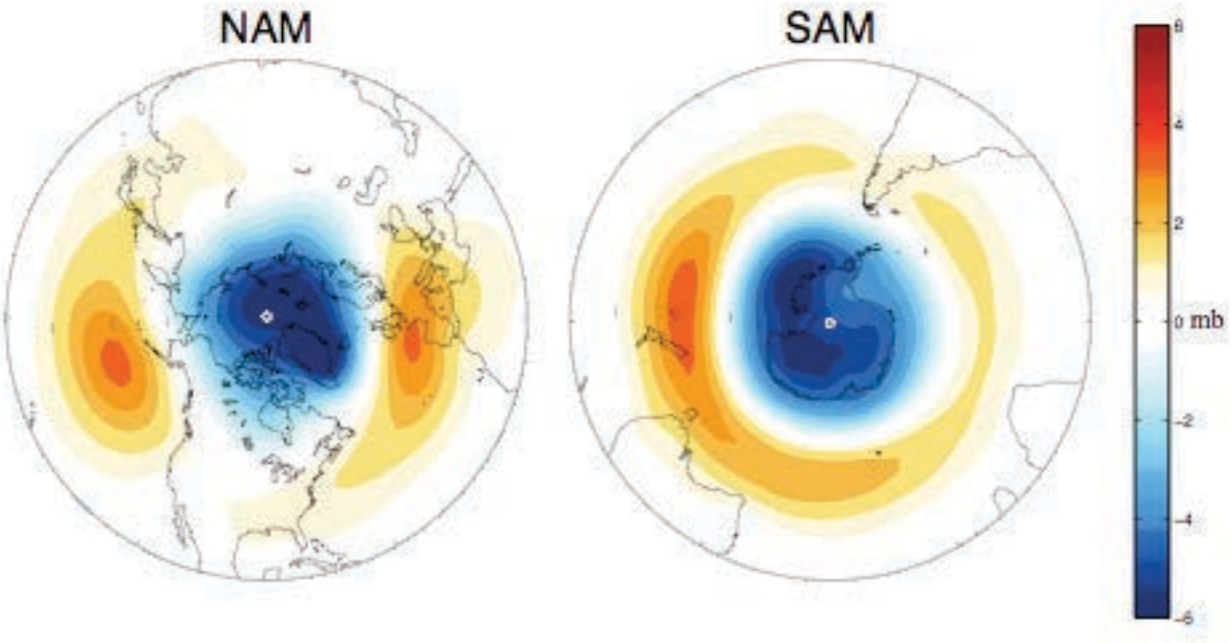

Figure 1.4 THE NCAR CCSM 1870 control 100 year annual NAM and SAM. The low [high] pressure over the poles [mid latitudes] marks the positive phase of the annular modes. Units are in mb.

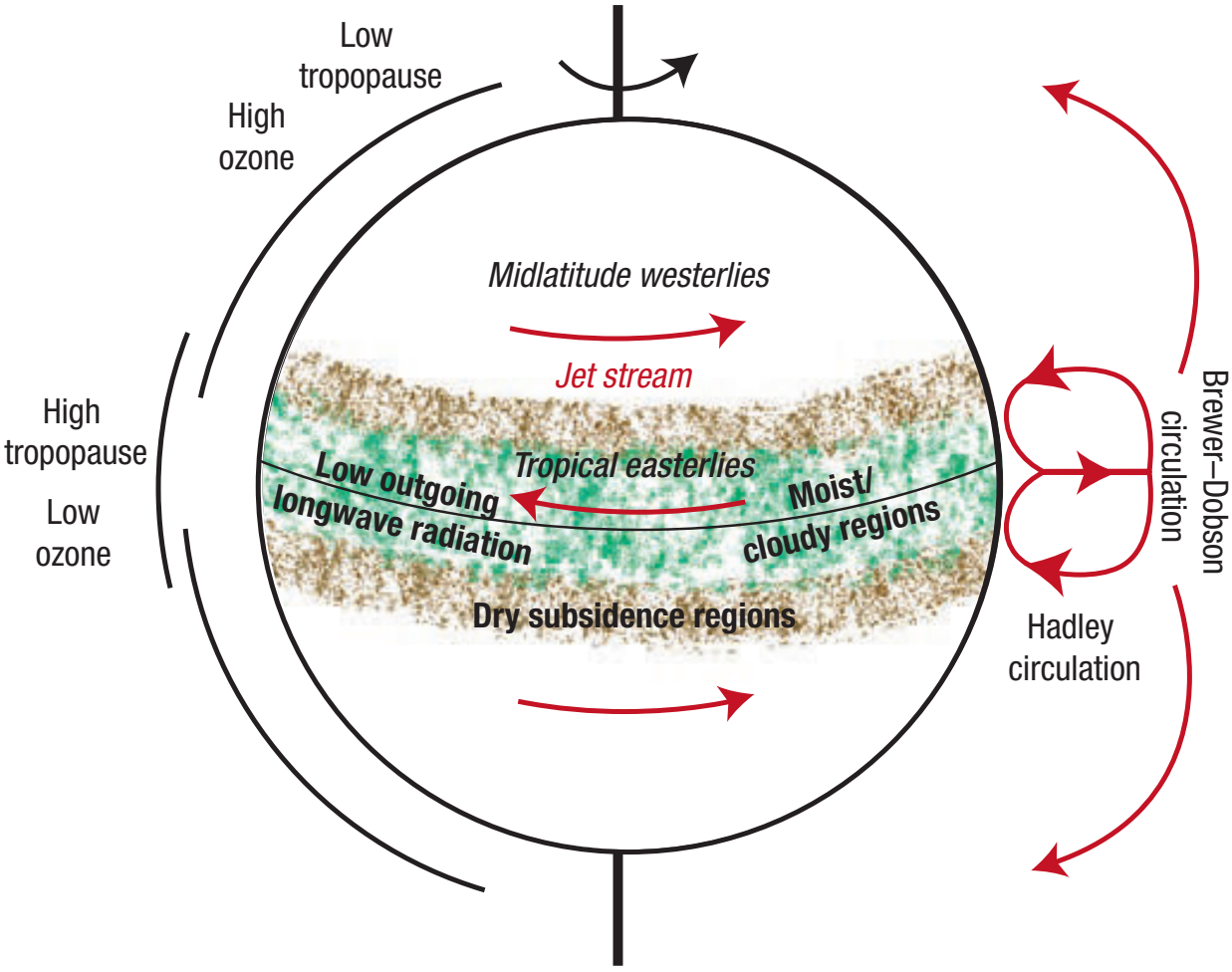

Figure 1.5 A schematic of the general circulation of the atmosphere. Taken from *Seidel et al., 2007*.

Chapter 2

Methods

2.1 NCAR CCSM Model

2.1.1 Future Climate Simulations

In this study, the model output from the NCAR CCSM3 40-member ensemble is used to estimate the spread of future climate trends. This ensemble was chosen because it is an initial condition ensemble, and it is a fully coupled climate model. The GCM contains a land (Community Land Surface Model version 3), ocean (Parallel Ocean Program version 1.4.3), atmosphere (Community Atmosphere Model version 3), and sea ice model (Sea Ice Model version 5), which allows it to simulate coupled aspects of the climate system [*Collins et al.*, 2006]. The model has a native spatial resolution of approximately 2.8˚ X 2.8˚ and the time domain spans 2000-2060. Output from the model is provided in monthly mean format.

The model is forced by the Special Report on Emission Scenarios (SRES) A1B forcing scenario. This particular forcing corresponds to rapid economic growth and moderate development of "green" technologies. The A1B forcing scenario assumes nations will cooperate on reducing greenhouse gas emissions and moderately apply climate change treaties. [*IPCC Special Report Emission Scenarios*, 2000].

Each realization of the CCSM model is produced by initializing the model with a different day between December 1999 and January 2000. By simply changing the initial conditions alone, the model produces a range of outcomes for any variable [*Madden*, 1976].

2.1.2 1870 Control Run

Data from the CCSM T42_gx1v3 1870 control simulation (1870 control) is used in this study. In this simulation, greenhouse gas concentrations remain fixed at 1870 levels. The control run has the same resolution as the 40-member ensemble, but the time domain is 200 years. The output from the control simulation is in monthly mean format.

2.2 Observations

Observed data was taken from the Hadley Center Hadcrut3 combined land and ocean surface temperature dataset. The resolution of the data is 5˚ X 5˚, and the data extends from 1850-present. In addition to the Hadcrut data, the NCAR sea level pressure data was also used. The data extends from 20˚N-90˚N, and has a spatial resolution of 5˚ X 5˚.

2.3 Derived Variables

Variables analyzed for this study include surface temperature, precipitation, indices of the annular modes jet latitude, and width of the tropics. The precipitation field and annular modes are the variables that require the most calculation to obtain. Because of this, their derivation will be discussed in detail.

2.3.1 Precipitation

The precipitation flux was not given in the native model output, so it was derived with an equation. The precipitation flux was calculated from the large-scale (stable) precipitation rate (PRECL) and convective precipitation (PRECC) rate with following the equation:

$$Precipitation\ Flux = (PREECL + PRECC) * \rho_{H20} \quad (1)$$

The units of the precipitation flux are Kg/m2s. Once the precipitation rate is calculated, it can be converted into yearly precipitation.

2.3.2 Annular Modes

The annular mode indices were calculated with the leading EOFs of the monthly sea level pressure field from latitudes 20N-90N. The calculation was performed by weighting the monthly mean sea level pressure anomalies by the square root of the cosine of the latitude, and then applying a principal component analysis to the covariance matrix. The first standardized principal component is the Northern Hemisphere annular mode. The summer (JJA) and winter (DJF) seasons were extracted from the monthly NAM index.

2.4 Calculating Significance

In this study, the trends are tested to see if they are significantly different from zero at the 95% confidence level. The equations used to calculate the threshold for significance were taken from *Santer* et al. 2000. A walkthrough of the equation is given below:

The least squares linear regression estimate of the time series is defined by equation (2), where *b* is the regression coefficient, or slope, of the regression line, and *t* is a time index.

$$\hat{x}(t) = a + bt; \quad t = 1, \ldots n_t \qquad (2)$$

The residuals of the linear regression are defined by equation (3), which is the regression line subtracted from the time series.

$$e(t) = x(t) - \hat{x}(t); \quad t = 1, \ldots n_t \quad (3)$$

In order to perform the significance test, the standard error of b must be known, and it is given in equation (4).

$$s_b = \frac{s_e}{[\sum_{t=1}^{n_t}(t-\bar{t})^2]^{1/2}} \qquad (4)$$

$$s_e{}^2 = \frac{1}{n_e - 2}\sum_{t=1}^{n_t} e(t)^2 \qquad (5)$$

In these equations, s_b is the standard error of b, s_e^2 is the variance of the residuals, and $\bar{t}$ is the mean of the time index. Equations (4) and (5) only work for statistically independent values of e(t). Since many variables in the climate system contain some memory, the values of e(t) are not always statistically independent from one another. This issue is addressed by using an effective sample size, which is given from equation (6). The equation uses the lag-1 autocorrelation (r_1) to correct for residuals that are not independent from one another. It should be noted that the r_1 terms in equation (6) are not squared in Santer et al., but the equations do not have any obvious effects on the results. Equation (6) squares the r_1 term to correct for a negative autocorrelation. Without the correction, a negative autocorrelation would increase the effective sample size.

$$n_e \approx n_t \frac{1 - r_1{}^2}{1 + r_1{}^2} \qquad (6)$$

In order for a trend to be significant, the value of t_b (given in equation 7) must exceeded the value of t_{crit}, which is found in a Student-t table with n_e degrees of freedom at a 95% significance level (two-tailed).

$$t_b = {}^{b}/_{s_b} \qquad (7)$$

In order to calculate the minimum trend for a time series to be significant,

$$t_b{}^* = t_{crit} \qquad (9)$$

Assuming all properties of the time series remain fixed, the minimum slope, or critical trend, can be calculated with the following equation:

$$b^* = t_b{}^* s_b \qquad (10)$$

This calculation only works for a single ensemble member, since the autocorrelation and standard error are different for each model. In order to take the other members into account, we use the largest critical trend for all members as the threshold for significance. Doing so implicitly assumes that all trends share the same variance, and poses a stricter value for most trends to be significant.

2.5 Statistical Models

2.5.1 Multiple Linear Regression

A multiple linear regression model is a statistical model that uses multiple independent variables (predictors) to estimate the value of a dependent variable. In this model, each independent variable is weighted by the linear regression coefficient of the dependent variable on each of the independent variables. A predictive model is formulated by summing all of the weighted independent variables.

The accuracy of a multiple linear regression model is inversely proportional to the amount of error in the model. A means of checking the fit of the multiple linear regression model to a dataset is to calculate the value of r^2. This value lies between 0 and 1, and higher values of r^2 indicate that the independent variables explain much of the variance in the dependent variables [*Spiegel and Stephens,* 1998].

In this study, a form of multiple linear regression is used to make predictions of surface temperature trends. We use the first 10 principal components of the sea level pressure fields as

predictors, and the surface temperature as the predicted variables. The leading 10 principal components are used, because they explain much of the variance of the surface temperature field. If fewer than 10 principal components are used, then the sea level pressure field will predict the variance in the surface temperature field less accurately. Conversely, if more than 10 principal components are used, the sea level pressure field will become a better predictor of the surface temperature field, but higher order principal components will be rendered "artificial" because they are more of a mathematical construct than a physical phenomenon. As a result, 10 principal components is subjective, but each principal component is likely to have some physical meaning, and collectively, they are fairly accurate in predicting the variance in the surface temperature field.

2.5.2 Autoregressive Process

An autoregressive models is a statistical model that produces a forecast based on the properties of the observed behavior. With this model, past observations are used to estimate current observations. Usually, this form of model uses a lag autocorrelation to preserve the memory in the data. Then, the memory is applied to a white noise time series. The governing equation for this model is given by equation (11).

$$x_t = \sum_{i=1}^{N} a_i x_{t-1} + \varepsilon_t \qquad (11)$$

In the equation, a_i is the lag autocorrelation, and ε_t is the value of the white noise time series at time *t*. This type of model is useful for this study, because many variables in the climate contain some memory [*Allen and Smith*, 1994]. This helps the AR1 model generate noise that is similar to the internal variability in the climate.

Chapter 3

Results Part I

3.1 Overview

3.1.1 Goal

The goal of this section of the research is to develop simple statistical models that can be used to derive an analytic solution or probability density function for the NCAR CCSM 40-member ensemble (CCSM model) trends. The analytic solution will be used to estimate the spread, or the dispersion, of the 40-member ensemble trends. The key benefit of using statistical models to estimate the ensemble spread is that statistical models are computationally inexpensive when compared to complex GCMs. As a result, these models allow for significantly larger ensembles to be created. Larger ensemble sizes can be used to make a more accurate assessment of how internal variability impacts future climate projections.

In this study, two classes of statistical models will be used to estimate the model-to-model dispersion in surface temperature predictions from the CCSM 40-member ensemble. Once the statistical models are developed, their output will be compared with each other and evaluated. The statistical model that gives the best estimate of the model-to-model dispersion in the 40-member ensemble will then be used to help assess the likelihood of future climate trends being significant.

3.1.2 Models Used

A total of three statistical models are developed with the intent of estimating the dispersion in the surface temperature projections from the 40 ensemble members. The first two

models are based on the variability of the atmospheric circulation. The first model uses the observed circulation and the observed temperature field to estimate the spread in trends of the 2000-2060 surface temperature field from the 40-member ensemble. The second model uses the circulation and temperature field from the CCSM control simulation to estimate the spread in trends from the 40 ensemble members. These *circulation models* were developed on the premise that variability in the atmospheric circulation drives much of the high-frequency variability in the surface temperature field. By assuming the amplitude of the circulation's variability will remain fixed in time, the models can be used to generate artificial time series of projected surface temperature [*Huntingford et al.,* 2013].

The third model creates artificial simulations of surface temperature from a lag-1 autoregressive process (AR1 model). The AR1 model is based on the variability in the CCSM control simulation. The AR1 model samples the noise or variability from a control simulation for any given variable, and constrains the future climate simulation to have the same variability and memory as the control simulation. Like the circulation models, the AR1 model is simple to run when compared to a GCM. In principle, it is possible for the models to simulate an infinite number of future simulations.

3.1.3 Variables and Domains

In this section of the study, the statistical models attempt to replicate the spread or uncertainty in the 2000-2060 surface temperature projections for the Northern Hemisphere cold-months (NDJFMA), in the NCAR CCSM 40-member ensemble. The surface temperature field was chosen because there is ample evidence that the atmospheric circulation influences the variability in the surface temperature field [*Deser et al.,* 2014]. This gives the best chance for the

circulation models to accurately replicate the dispersion of the surface temperature trends. The cold months were chosen because the variability and the spread in the surface temperature trends is highest during this time. Secondly, the circulation is more vigorous during the winter months. The time domain of this study is limited to 2000-2060 because it is the time domain of the NCAR CCSM 40-member ensemble.

For this study, we will focus on surface temperature time series over three regions: the Northern Hemisphere, Canada, and Siberia (Figure 3.1). The latter locations have a high amount of variability in the surface temperature field and are very sensitive to changes in the atmospheric circulation. Reasons for choosing these domains will become more apparent throughout the following text.

3.2 CCSM Model Output

The surface temperature time series for the CCSM Northern Hemisphere, Canada, and Siberia domains are shown in the left column of Figure 3.2. The gray lines represent the 40 individual ensemble members, and the black line represents the ensemble mean. The output from the CCSM model shows a robust response to the A1B forcing scenario. In this scenario, the anthropogenic forcing is nonlinear, and the steady increase in CO_2 concentrations begins to accelerate around 2050. In spite of the nonlinear anthropogenic forcing, the model's response to the forcing is very close to linear and remains consistent throughout the time domain. Of the three domains studied, the Northern Hemisphere shows the least amount of noise and the clearest anthropogenic signal. As expected, Siberia and Canada are substantially noisier than the Northern Hemisphere. Due to the higher amplitude of noise on regional scales, the anthropogenic signal on regional scales is not as evident as the signal on hemispheric scales.

For all domains studied, all of the ensemble members show a warming surface temperature trend. It is important to note that the variability in the time series is fairly consistent across all ensemble members. This means that the amplitude of the noise differs by an insignificant amount from one ensemble member to the next. Further, the amplitude of the internal variability remains fixed in time. Spatially, the surface temperature warming displays a familiar pattern, in the sense that the warming trends are greater over land, and the warming is generally larger relatively smaller spatial scales. Maybe add another figure.

The noise generated by the CCSM model can amplify or reduce the simulated trends. When considering all ensemble members, the model's response has a range and spread of possible trends. The range is the difference between the largest and smallest trend, while the spread is the standard deviation about the mean trend. The range of trends suggests that local and regional scales can warm within a range of nearly 3˚K over the first half of the 21st century. For reference, the left column of Figure 4.3 shows the strongest and weakest trends for each domain studied in the CCSM model.

3.3 Circulation Models

3.3.1 Motivation

This study uses two separate circulation models to replicate the surface temperature field from the CCSM model. The circulation models are of interest because they test whether the circulation can account for the spread in the 40-member ensemble's surface temperature field. The first circulation model uses the observed circulation from the NCAR sea level pressure dataset and the observed surface temperature field from the HadCRUT dataset. The second circulation model is built with the 1870 CCSM control circulation and temperature field. Of the

two circulation models, the second model is better suited to estimate the 40-member ensemble spread, because it uses the CCSM model's circulation to describe the CCSM model's surface temperature field.

As stated previously, the purpose of the circulation models is to use the variability in the atmospheric circulation to estimate the dispersion, or spread, in the 40-member ensemble surface temperature field. In theory, these models should work because the monthly mean surface temperature field is strongly linked to the variability of the atmospheric circulation in both observations and models [*Wallace et al.,* 1996; *Daithi and Andrew,* 2001; *Deser et al.,* 2014].

The relationship between the circulation and surface temperature field is shown in Figures 3.4 and 3.5. In the figures, leading sea level pressure EOFs are contoured, and the shading shows the regression of the surface temperature field onto standardized values of the leading PCs. All of the panels from both figures show distinct shading patterns over landmasses. These results indicate that the atmospheric circulation influences local and regional temperature, as opposed to hemispheric mean temperature [*Quadrelli and Wallace,* 2004].

Figures 3.6 and 3.7 show maps of the coefficient of multiple correlation (r^2) between the atmospheric circulation and the surface temperature field in the observations and the CCSM control data. The coefficient of multiple correlation is the ratio of the variance in the surface temperature explained by PCs 1-n over the total variance in the surface temperature field. r^2 is calculated with the following equations:

$$s_n = s_1\sqrt{1 - {r^2}_{12} - {r^2}_{13} \ldots - {r^2}_{1n}} \qquad (12)$$

$$r_{temp.PC} = \sqrt{1 - \frac{{s_n}^2}{{s_1}^2}} \qquad (13)$$

Where n is the nth PC, s_1 is the standard deviation of the surface temperature time series, and r_{1n} is the correlation coefficient of the surface temperature time series and the nth PC. It is important to note that these equations have been simplified because of the orthogonality of the PCs.

Areas with high values of r^2 for the PC 10 panel suggest that the circulation explains much of the variance in the surface temperature field. Both of the figures indicate that the circulation explains a large portion of the variance in the surface temperature field over central Canada and Siberia. Physically, the variability in the atmospheric circulation correlates strongly with surface temperature at these locations. This is because these locations are over the land (low heat capacity) and they are susceptible to warm/cold air advection [*Serreze et al.,* 2011]. Over the oceans, the control simulation underestimates the relationship between the circulation and temperatures over the oceans, but it is unclear why this happens.

Calculations reveal that during the cold months, the observed circulation can explain up to 75%, 60%, and 57% of the variance in the observed surface temperature field over Siberia, Canada, and the Northern Hemisphere, respectively. Similarly, the control circulation can explain 78%, 74%, and 51% over Siberia, Canada, and the Northern Hemisphere, respectively. Since the highest correlations are over Siberia and Canada, these locations and the Northern Hemisphere will be the domains used in this study.

3.3.2 Circulation Model Using Observations

The circulation model was developed by fitting the first 10 PCs of the sea level pressure field to the surface temperature time series. This was accomplished by regressing the NCAR 1958-2013 observed sea level pressure field onto the Northern Hemisphere, Canada, and Siberia 1958-2013 HadCRUT surface temperature time series. This operation yields 10 regression

coefficients, α, for each domain, and *n* is the regression coefficient for the nth PC. After determining the regression coefficients, ten artificial red noise PCs (denoted PC^*_n) were created for each domain. The ten red noise PCs prescribed to have the same memory and standard deviation as the observed standardized PCs, which makes for a better representation of the realizations of the NCAR-40 member ensemble. Additionally, the length of the PC^*_ns corresponds to the time domain of 2000-2060. The PC^*s were then multiplied by their corresponding regression coefficient. For each of the domains, the products of the PC^*_ns and the regression coefficients were summed together, and created the artificial climate noise represented in equation (14).

$$climate\ noise = \sum_{n=1}^{10} \alpha_n PC_n^* \qquad (14)$$

The regression coefficients (α_n) are plotted in Figure 3.8. The surface temperature projection for 2000-2060 is calculated by adding the climate noise onto the anthropogenic forcing. The ensemble mean of the CCSM model represents the anthropogenic forcing. The surface temperature projection is represented by equation:

$$T_{2000-2060} = ensemble\ mean + climate\ noise \qquad (15)$$

With the use of equations (14) and (15), 40 projected surface temperature time series were generated for each domain. The results of the multiple linear regression model with the observations are shown in the center column of Figure 3.2 check this number.

3.3.3 Circulation Model Initialized Using Control Data

The circulation model based on the CCSM control data was created in an analogous manner as the model with observations. The only difference between the two circulation models is that the NCAR observed sea level pressure field was replaced by the 200 year CCSM 1870

control sea level pressure field, and the HadCRUT observed surface temperature data was replaced with the 200 year 1870 CCSM control surface temperature field. Even though the time domain in the control data is longer than the time domain in the observations, no widespread changes to methods needed to be made because the length of the time domain does not alter the relationship between the circulation and the surface temperature field. The 1870 control surface temperature data was detrended to remove small amounts of climate drift within the CCSM model.

In addition to the differences in the time domain, the control data is slightly different from the observations. The control data has higher resolution, fewer missing data points, and the temperature trends are slightly different from the observation. As a result, the multiple linear regression model with the control data has different regression coefficients than the multiple linear regression model with the observations (Figure 3.9).

3.4 AR1 Model

3.4.1 Motivation

The AR1 model was developed as a means of replicating the dispersion of the 40-member ensemble temperature trends with a single control simulation. The AR1 model is based on the noise from the CCSM control run. The model simulates noise from the control run and adds the noise onto the CCSM ensemble mean. This constrains the climate simulation from 2000-2060 to have the same variance and noise as the control run. Since there are no iterative processes or physics in the model, it is computationally inexpensive to run.

3.4.2 Constructing the AR1 Model

The AR1 model for the surface temperature field was created by first extracting the cold month surface temperature time series from the CCSM 1870 control simulation for the Northern Hemisphere, Canada, and Siberia. The memory and standard deviation was then taken from the detrended time series over the three domains. The time series was detrended to remove any existing amount of climate drift from the control run. Next, 40 red noise time series were created for each of the three domains. Each red noise time series has a mean of zero, and it has the same standard deviation and memory as the control simulations in its respective spatial domain. All of the artificial red noise time series span 2000-2060.

The surface temperature projections for 2000-2060 were created by adding the three sets of red noise time series onto the CCSM ensemble mean time series for the Northern Hemisphere, Canada, and Siberia domain, respectively. The surface temperature projection is represented by the equation:

$$T_{AR1\ 2000-2060} = ensemble\ mean + climate\ noise \quad (16)$$

The output from the AR1 model is shown in the right column of Figure 3.2

3.5 Model Results

The goal of these simple statistical models is to estimate the spread in the CCSM 40-member ensemble surface temperature field. When assessing the spread of the models, the circulation and AR1 models were extended to 1000 realizations. Increasing the ensemble members of the statistical models causes the surface temperature trends to take on a normal distribution. The spread in this distribution remains fairly constant with each model run. When the statistical models are run with 40 realizations, the trends fail to take on a normal distribution,

and the spread changes with each run because of the small sample size. The trends from the statistical models are in units of K/decade and the standard deviation of the trends for all models is summarized Table 3.1.

3.5.1 Statistical Model Results

Both of the circulation models produce a spread of surface temperature trends that are similar to the CCSM model. For each of the multiple linear regression models used in this study, the trends have a narrower spread over the Northern Hemisphere, and the spread increases over Siberia and Canada. However, the circulation model with observations performs better on the hemispheric scale, while the circulation model with the CCSM control data performs better on regional scales. The observations perform better on the hemispheric scale, which is consistent with the observations' higher r^2 values over the Northern Hemisphere. It is likely that the CCSM model does not fully capture the relationship between the atmospheric circulation and surface temperatures over the ocean. Because of this, the circulation model based on the control data may not be accurate over the ocean, which results in poor performance on the hemispheric spatial scale. The cause of the CCSM model's underperformance over the ocean is not certain, and investigating this cause goes beyond the scope of this research.

Like the circulation models, the AR1 model produces a spread of trends that resemble the CCSM model. The output from the AR1 models differs from the circulation models, because the AR1 model is constrained in such a way that it shares many of the same properties as the CCSM model. In particular, the AR1 model has the same noise as the CCSM model. Additionally, individual realizations of the AR1 model preserve the same variance as the realizations in the

CCSM ensemble. Because of these constraints, the AR1 model faithfully reproduces the spread of uncertainty across all three spatial domains studied.

3.5.2 Comparison of Circulation and AR1 Model

In this study, the AR1 model performs better than both of the circulation models by capturing more of the spread in the surface temperature from the CCSM model. Not only does the AR1 model better capture the spread and amplitude of the CCSM model, the realizations of the AR1 model possess the same memory as the realizations in the CCSM model. The circulation models do not fully account for the memory in the CCSM model, but simply produce random time series that loosely resemble the realizations of the CCSM model. Overall, the realizations of the circulation models do not share the same properties as the realization in the CCSM model. This hinders the circulation models' ability to create the spread in the CCSM model's trends. Because of these deficiencies in the circulation models, it is impossible for either of the circulation models to perform better than the AR1 model.

In summary, the AR1 model is a better tool for assessing the uncertainty in climate predictions. The circulation explains the bulk of the variance in the surface temperature field, which makes the circulation models a viable substitute. However, better results can be obtained from the AR1 model. For these reasons, the AR1 model will be used to assess the uncertainty and significance of other parameters in the latter section of this study.

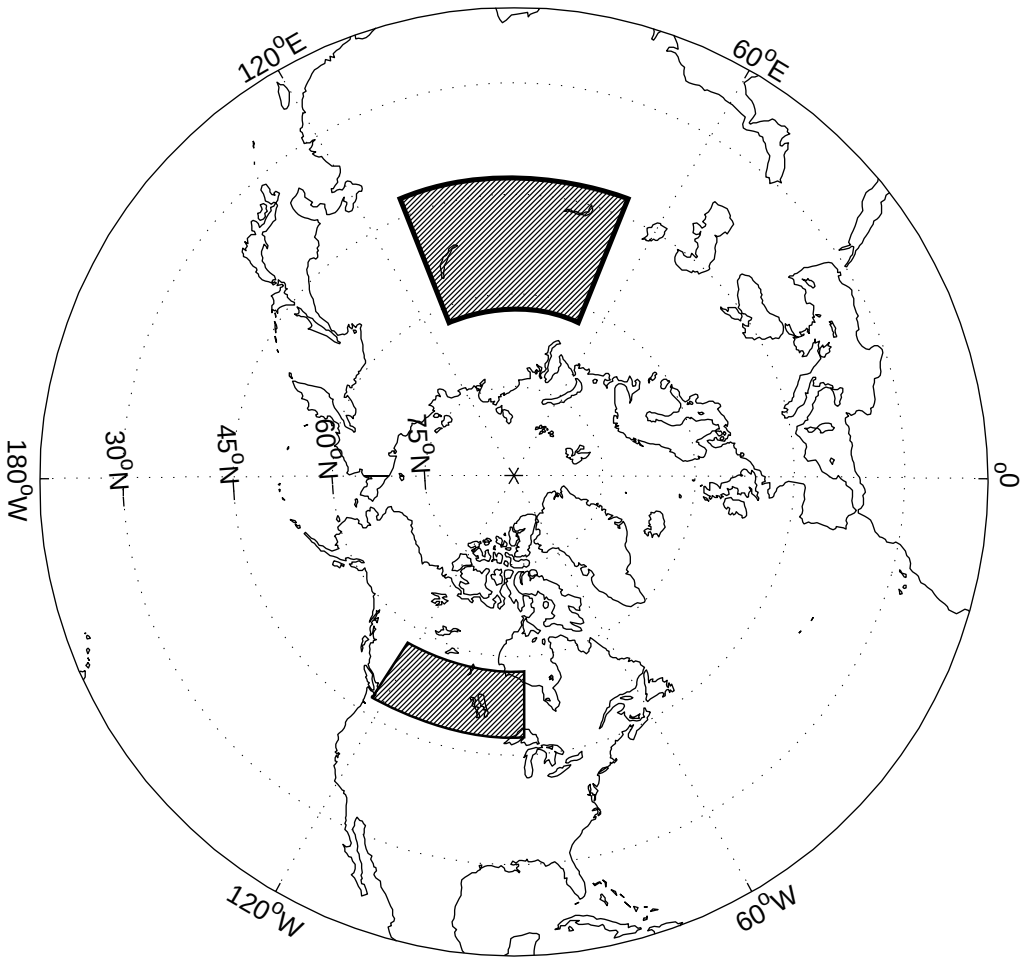

Figure 3.1 The hatched regions show the Canadian and Siberian domain used in the study

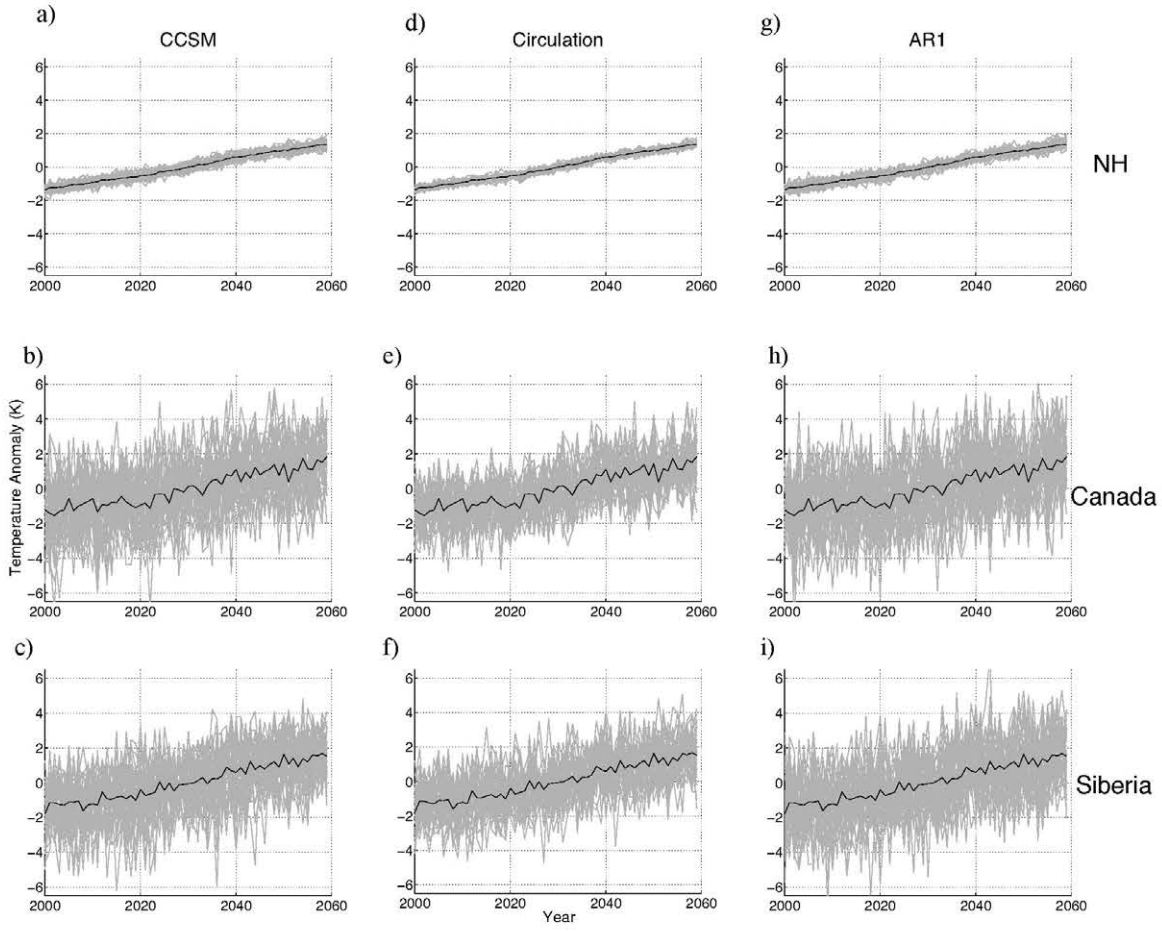

Figure 3.2 Surface temperature time series for the CCSM model, multiple linear regression model with observations, and the AR1 model, for the Northern Hemisphere, Canada, and Siberia domains. Gray lines represent 40 individual realizations of the models, and the black line represents the CCSM ensemble mean or anthropogenic forcing.

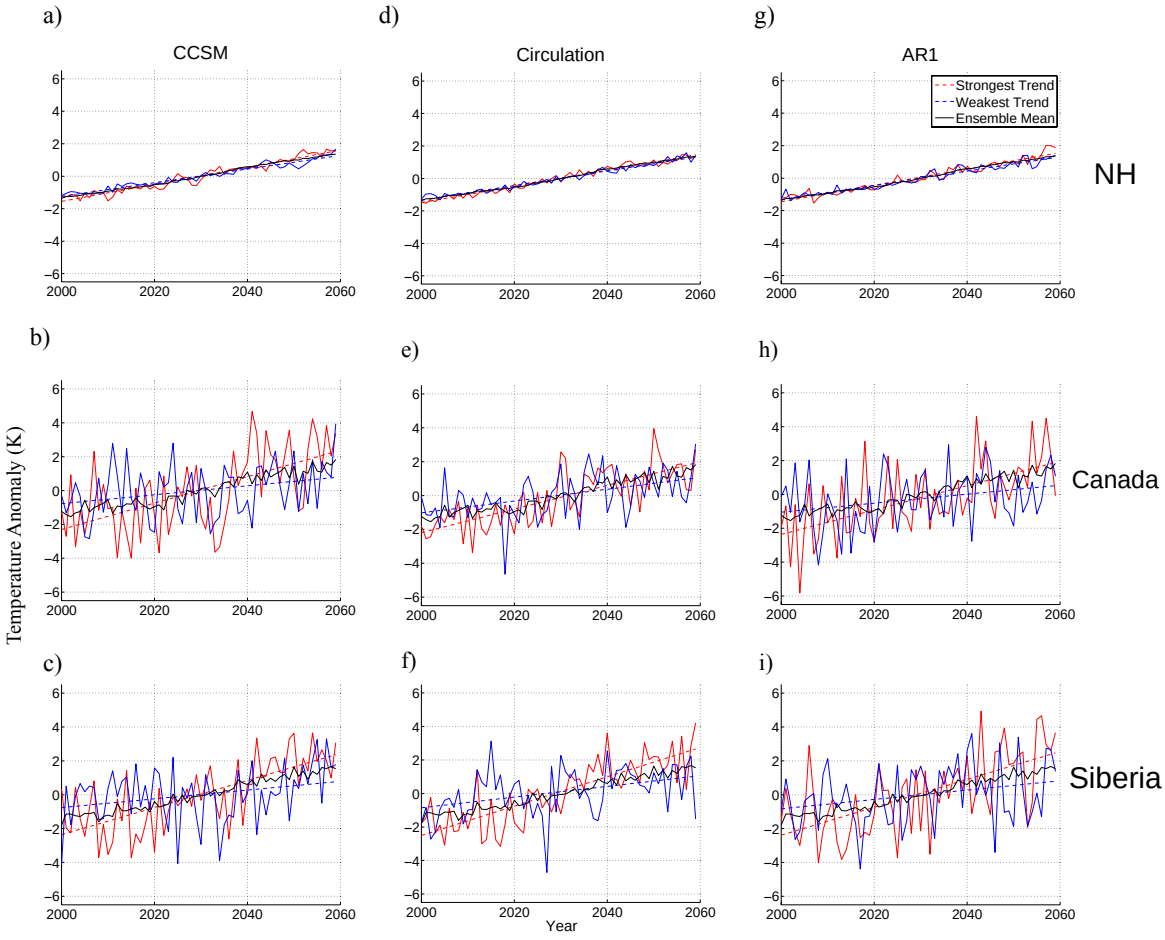

Figure 3.3 Surface temperature time series with the weakest and strongest trend in the CCSM, AR1, and circulation models for the Northern Hemisphere, Canada, and Siberia domains

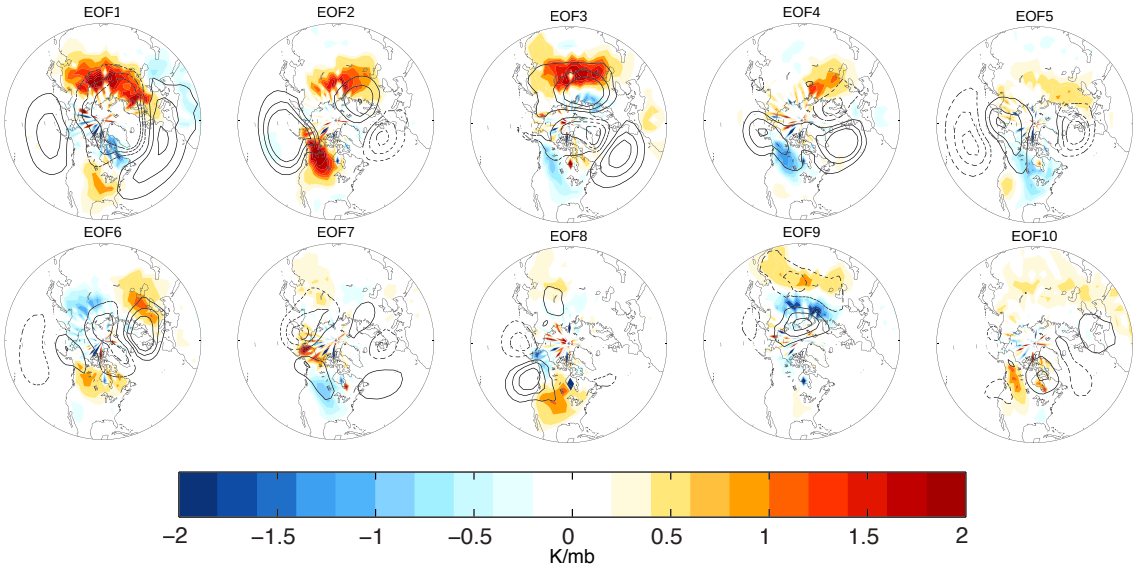

Figure 3.4 Sea level pressure and surface temperature regressed onto the first ten principal components of the sea level pressure field. Solid/dashed contours show positive/negative sea level pressure anomalies (contour interval 1mb). Shading shows the surface temperature regressed onto the PCs.

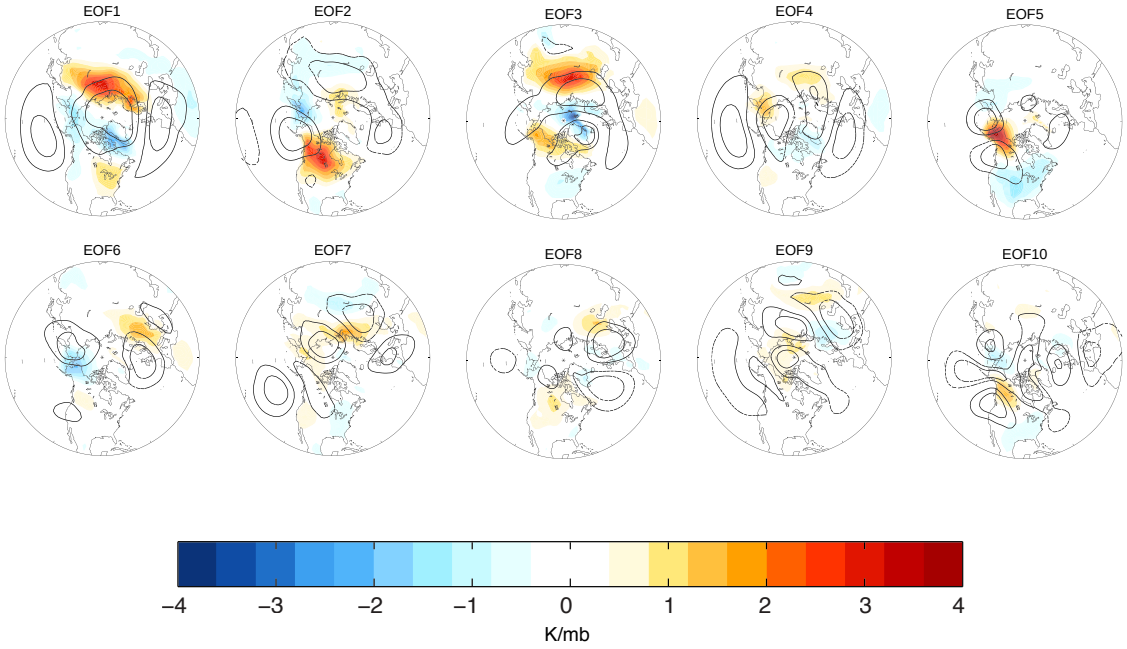

Figure 3.5 As in Figure 3.4. but for the CCSM control sea level pressure and HadCRUT temperature data

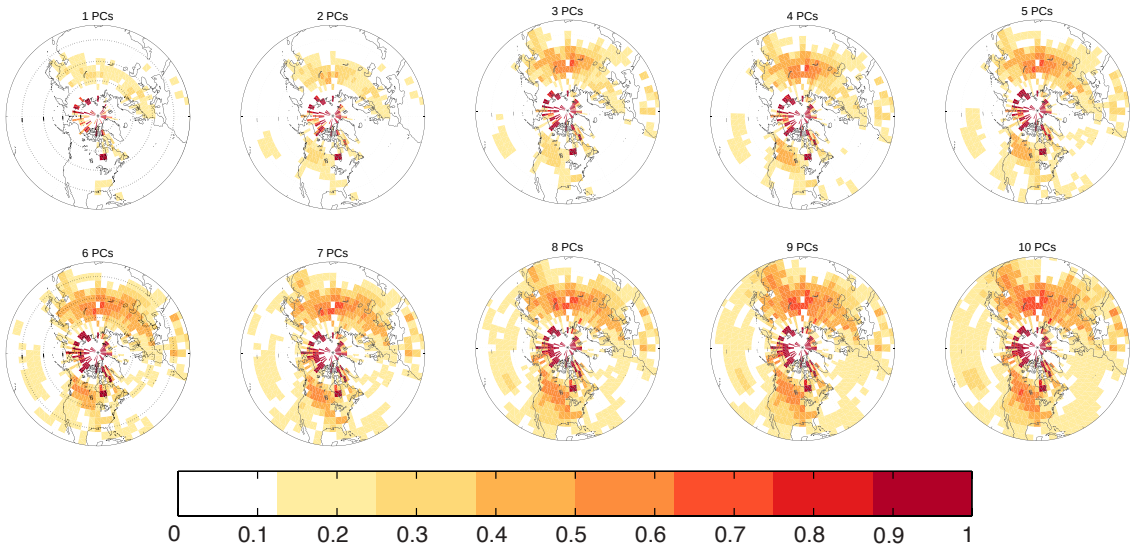

Figure 3.6 Maps of the coefficients of multiple correlation between the observed circulation and surface temperature. X PCs denotes the multiple correlation between PCs 1-X of the sea level pressure field and the surface temperature field.

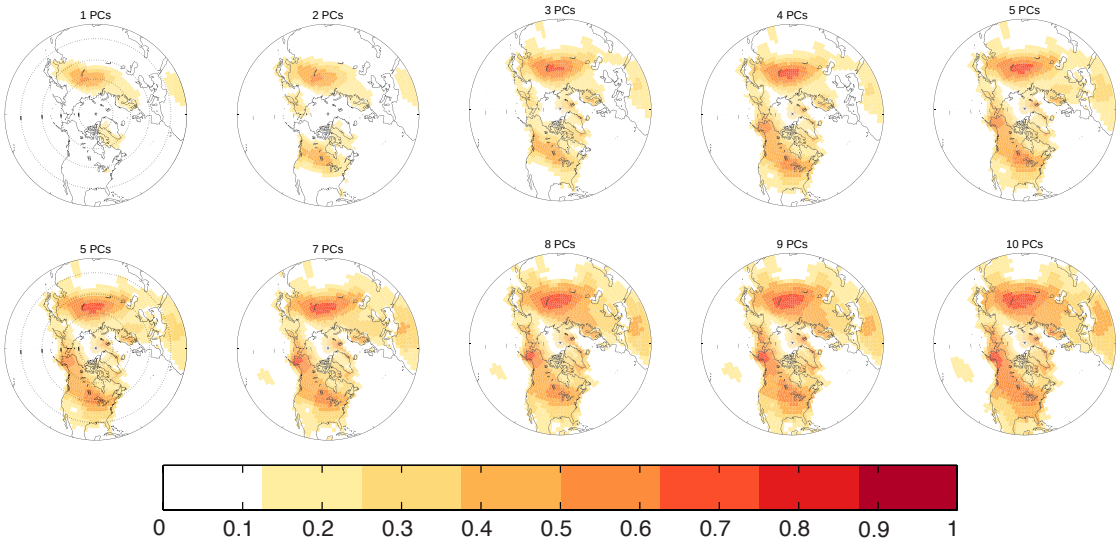

Figure 3.7 As in Figure 3.6 but for the control simulation

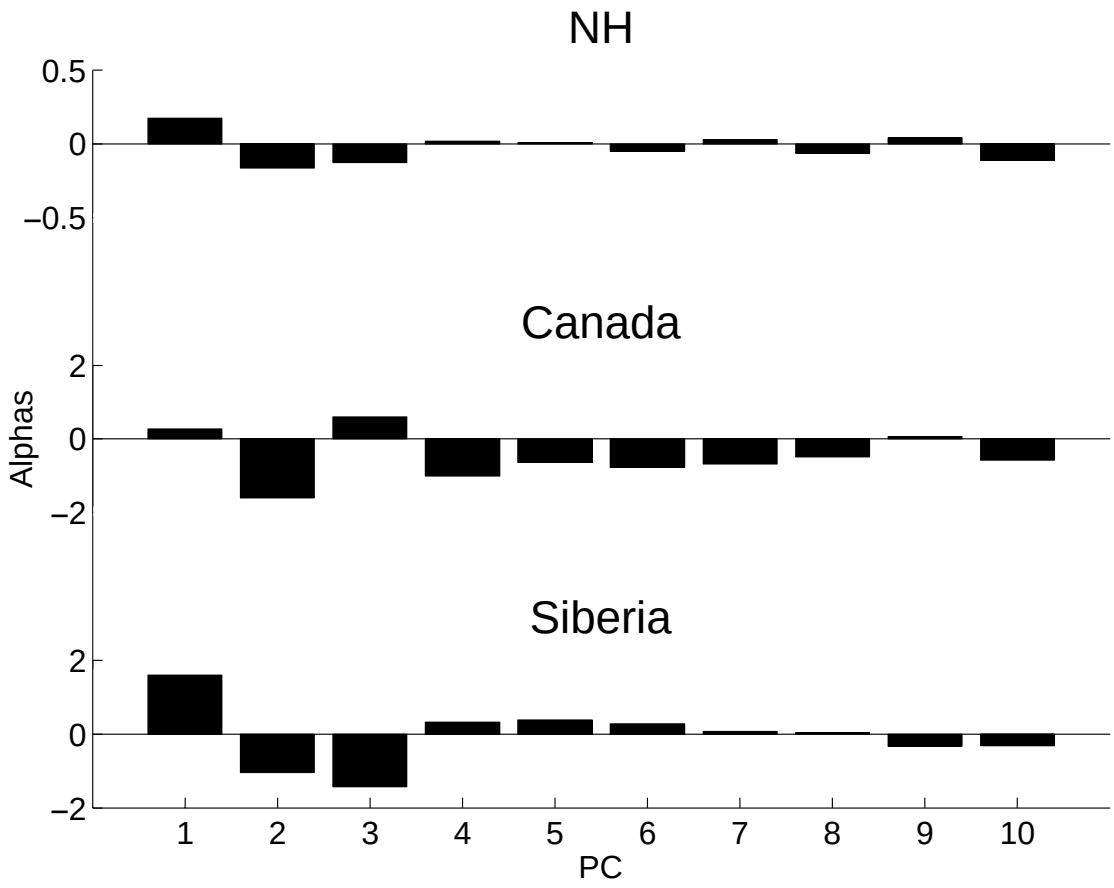

Figure 3.8 Regression coefficients between the leading PCs of the observed sea level pressure field and observed surface temperature for the domains studied.

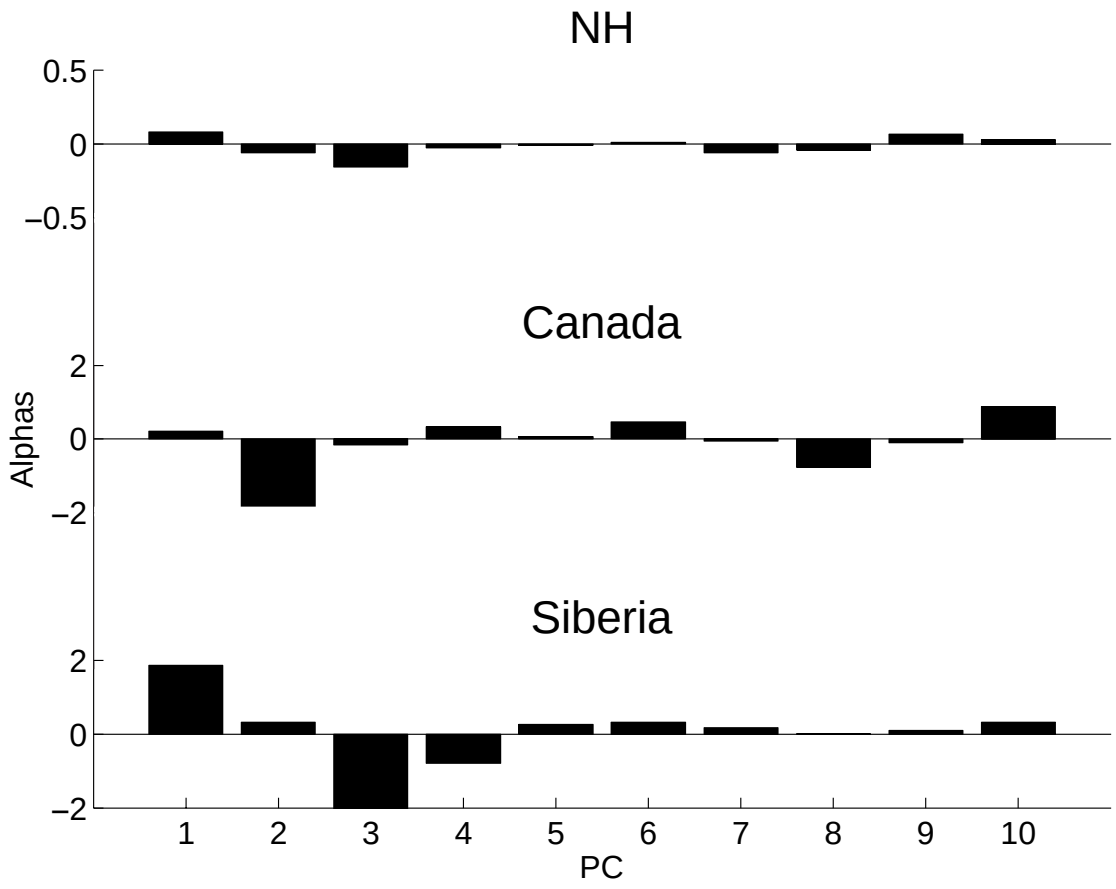

Figure 3.9 As in Figure 3.8 but for the control simulation

Table 3.1 The spread (standard deviation) of the surface temperature trends for the CCSM model, circulation model based on observations, circulation based on CCSM control data, and the AR1 model. Units are in K/decade.

Model Spread in Standard Deviation				
	NCAR-CCSM	Observations	Control Data	AR1
NH	0.026	0.012	0.008	0.017
Canada	0.133	0.090	0.111	0.131
Siberia	0.121	0.093	0.114	0.120

Chapter 4

Results Part II

4.1 Overview

4.1.1 Goal

The primary goal of this section is to use the 40-member ensemble to estimate the likelihood that future climate trends will be statistically significant from zero at the 95% confidence level. In chapter 3, we used the CCSM control surface temperature field to determine that the AR1 model is a better tool than the two circulation models for assessing the uncertainty in the CCSM ensemble. In this chapter, we assess the likelihood of significant trends in the surface temperature field, precipitation field, and atmospheric circulation over the period of 2000-2060.

4.1.2 Models Used

This section utilizes output from the CCSM 40-member ensemble, and 1000 realizations from a lag-1 autoregressive model (AR1). The AR1 model is used to create 1000 realizations of the future climate that are based on the statistical characteristics of the CCSM control run. In principal, the AR1 model can be solved analytically to provide estimates of all possible future trends in the CCSM model. In practice, it is assumed that 1000 realizations are enough to estimate the analytic solution. For the context of this study, the solutions will be represented as probability density functions of the trends.

4.1.3 Model Spread and Significance

This section of the study evaluates the spread of the trends that are generated by the CCSM and AR1 models. Here, the model, or ensemble spread, is defined as the standard deviation of the trends about the ensemble mean trend. Since all models have the same forcing in this study, the amplitude of the climate's internal variability dictates the model spread. Hence, parameters and regions that are subject to large amplitudes of internal variability will have a larger spread. The model spread is an important attribute because it represents how much the internal variability can affect predictions of future climate.

In addition to the model spread, this section of the study will evaluate the trends of the CCSM model and determine if they are likely to be statistically significant from zero at the 95% confidence level. In order for a trend to be statistically significant from zero, it must exceed a certain critical value, or threshold for significance. The critical value is a function of the month-to-month variance and the magnitude of the trend in the model simulation. Details of the significance test are discussed in chapter 2. It is important to note that critical value of the trends assumes all of the ensemble members have the same variance (the assumed variance is the highest value of the variance from the detrended time series from all ensemble members). By assuming members have the same variance, the critical value for significance is higher and we are able to make an estimation of the threshold for tends to be significant. Without this assumption, the critical value would be lower, and the threshold for significance becomes less stringent.

Not only are individual ensemble members tested for significance, but so is the ensemble mean. Since the ensemble mean filters out the climate noise, there is less variance in the time series. As a result, the critical value for the ensemble mean trend in a given parameter is much

lower than it is for individual ensemble members. Under some circumstances, it is possible for the ensemble mean to be significant, while the individual ensemble members are not significant. In this case, the forcing is significant, but simulations of the climate are not significant.

4.2 Surface Temperature

On large spatial scales, the surface temperature trend is dominated by the anthropogenic signal. All GCMs that are forced with the SRES A1B scenario show a warming trend that is significantly different from zero on the global scale [IPCC 4th assessment report]. However, the magnitude of local and regional surface temperature trends varies spatially. In addition, local temperature trends exhibit higher amounts of variability than larger scale trends. This causes the trends to display a larger spread, which leads to them being less certain (Figure 5.1).

In this section, the surface temperature projections are evaluated over the Northern Hemisphere, the Arctic region, and Colorado. The trends are evaluated for the winter (DJF) months. These months were chosen because the variability in the surface temperature field is highest during this time.

4.2.1 Northern Hemisphere

The Northern Hemisphere was chosen because the surface temperature trends have been shown to be robust across many climate models [IPCC 4th Assessment Report, *Knutti and Sedláček*, 2012]. In addition, the amplitude of the internal variability is smaller on larger scales. As a result, the Northern Hemisphere surface temperature time series should be less affected by the internal variability than the Arctic or Colorado.

The CCSM and 1000-member AR1 Northern Hemisphere mean surface temperature time series are shown in Figure 5.2. The left panel shows the surface temperature time series for all 40 members of the CCSM ensemble. The gray lines represent each CCSM ensemble member, while the black line represents the ensemble mean.

The right panel of Figure 5.2 shows a normalized histogram (area under the distribution is 1) of the CCSM Northern Hemisphere temperature trends (gray boxes). Because of the normalization, values on the y-axis are dimensionless. The black line shows a normalized fit of the AR1 ensemble trends, which is an estimate of the analytic solution to distribution of surface temperature trends. The red lines represent the critical value, or significance threshold, for an individual ensemble member, and the green line represents the critical value, or significance threshold, for the CCSM ensemble mean (refer to Chapter 2 for more details). If the surface temperature trend for a single ensemble member exceeds the red line, then the trend is statistically significant from zero. If the ensemble mean of the CCSM model exceeds the green line, then it is significant.

The mean and standard deviation of the trends in the CCSM and AR1 model is 0.51 K/decade, and 0.03 K/decade, respectively. The two models share the same ensemble mean trends by construction. Additionally, both models share the same spread and skewness. These results show that the distribution of trends closely match the analytic solution produced by the AR1 model.

In addition to graphically displaying the mean and spread of the surface temperature trends in the two models, the right panel of Figure 5.2 shows that all of the trends in the CCSM and AR1 model are positive and significant (as indicated by the light gray text in the lower left of

the plot). Because all possible realizations are significant, the Northern Hemisphere surface temperature warming is likely to be statistically significant from zero in the future.

4.2.2 Arctic

Like the Northern Hemisphere, the warming of the Arctic region (60˚N-90˚N) has been shown to be robust across numerous climate models. The Arctic region is of interest because it is subject to the strongest warming trends anywhere on the globe (Figure 5.1). As seen in panel b of Figure 5.1, the standard deviation values are relatively high over the Arctic. This indicates that the Arctic mean surface temperature has more climate noise than the Northern Hemisphere mean surface temperature.

Figure 5.3 is the same as Figure 5.2, except the domain is the Arctic. Like the Northern Hemisphere surface temperature trends, the CCSM and AR1 Arctic surface temperature trends are positive and significant. The mean of the trends from the CCSM model is 1.07 K/decade, with a spread of 0.09 K/decade. The AR1 ensemble also has a mean of 1.07 K/decade, and a spread of 0.10 K/decade. The distribution of trends produced by the CCSM model closely resembles the distribution produced by the AR1 model. In this instance, the CCSM model produces a normal distribution with 40 realizations, and all realizations show significant warming.

4.2.3 Colorado

Unlike the Northern Hemisphere and the Arctic, Colorado represents a small domain. Subsequently, the surface temperature field over Colorado is much noisier than the Northern Hemisphere and Arctic surface temperature field. Colorado was chosen to represent an arbitrary

location over the globe. The output from the CCSM model suggests that Colorado will experience a warming trend slightly greater than zero, but the trend will be shrouded by large amounts of internal variability.

Figure 5.4 is the same as Figure 5.2, except the domain is a single grid point over Colorado. Like the other surface temperature domains, the CCSM and AR1 surface temperature trends over Colorado are constrained to share the same mean. The mean of the trends from the CCSM and AR1 model is 0.33 K/decade. This result implies that it is more likely for the surface temperature to display a warming trend than a cooling trend in the future climate.

The spread of the CCSM and AR1 model is 0.12K/decade and 0.18K/decade, respectively. Since the spread or standard deviation of the surface temperature trends is larger over Colorado than the Northern Hemisphere and the Arctic, the trends in the surface temperature field are less certain over Colorado than they are for larger spatial scales. In addition, the AR1 model generates a larger spread than the CCSM model. This is because the CCSM produces 40 random trends, and the trends happen to be fairly consistent with one another. This result does not compromise the accuracy of the AR1 model, but it suggests that 40 realizations from the CCSM model may not be enough to fully capture the spread of the trends.

In terms of significance, the CCSM model produces a significant ensemble mean, but 55% of the ensemble members are significant. Similarly, the AR1 model suggests 56% of the realizations will be significant. The two models' results suggest that it is more likely than not that Colorado will experience a significant increase in surface temperature.

4.3 Precipitation

In the long-term mean, the largest amount of total annual precipitation is in the deep tropics, while the boundary of the extratropics receives the least amount of annual precipitation. The majority of coupled climate models predict that the deep tropics will receive more precipitation, while the extratropics will receive less precipitation [*Polade et al.,* 2014].

This section evaluates how well the AR1 model captures the spread of the CCSM model, and how likely the annual precipitation trends are to be statistically significant over the deep tropics (15˚N-15˚S), the subtropical Northern Hemisphere (45˚N-15˚N), and the subtropical Southern Hemisphere (15˚S-45˚S). The annual precipitation field was chosen because the CCSM trends showed little seasonality in the domains studied.

4.3.1 Subtropical Northern Hemisphere

The subtropical Northern Hemisphere domain (45˚N-15˚N) was chosen because the annual precipitation is expected to lessen over the 21st century (Figure 5.5). If drying is to occur between these latitudes, it can greatly affect a large amount of the human population. Therefore, it is important to understand how precipitation may change in this region.

The subtropical Northern Hemisphere zonal mean precipitation field shows a weak response to the anthropogenic warming and is shown in the left panel of Figure 5.6 (Figure 5.6 follows the same format as Figure 5.2). The right panel of Figure 5.6 shows that all of the annual precipitation trends are close to zero in the CCSM and AR1 model. The mean of the subtropical Northern Hemisphere precipitation trends from both the CCSM and AR1 model is 5.1e-4 mm/m2/decade. Additionally, the AR1 model roughly shares the same spread as the CCSM model.

In terms of significance, all projections suggest that the subtropical Northern Hemisphere will not experience any significant changes in precipitation. This is because the right panel of Figure 5.6 shows none of the CCSM or AR1 realizations to be statistically significant, nor the ensemble mean. Assuming the model is correct, it is improbable for the subtropical Northern Hemisphere zonal mean precipitation field to undergo a significant change in the future.

4.3.2 Subtropical Southern Hemisphere

Since this study addresses the subtropical Northern Hemisphere and deep tropics, the annual precipitation in the subtropical Southern Hemisphere (15˚S-40˚S) is evaluated for completeness. In addition, the reasoning and techniques used to study the subtropical Northern Hemisphere precipitation field is applied to the subtropical Southern Hemisphere.

When comparing the results of the subtropical Northern and Southern Hemispheres, the left panel of Figure 5.7 indicates that the subtropical Southern Hemisphere zonal mean precipitation field has a clearer anthropogenic signal than the subtropical Northern Hemisphere. In spite of the clearer response, the subtropical precipitation trends have a larger spread in the Southern Hemisphere (right panel of Figure 5.7).

Despite the larger spread in the subtropical Southern Hemisphere, the AR1 model produces a distribution of precipitation trends that closely resemble the distribution created by the CCSM model. By construction, the models share a mean trend of -0.01 mm/m2/decade, but the CCSM and AR1 spread is 2.5e-3 mm/m2/decade and 2.8e-3mm/m2/decade, respectively. As for significance, it is likely that the Southern Hemisphere will show significant drying. The CCSM model suggests that the ensemble mean will be significant, as well as 90% of the

members in the CCSM model. The AR1 model agrees with these results and suggests that 94% of the realizations will be significant.

4.3.3 Deep Tropics

The deep tropics were chosen because the annual precipitation trends have been shown to be consistent across many climate models. In addition, the anthropogenic signal to noise ratio in the deep tropics is higher than in the subtropics [*Hawkins and Sutton,* 2010]. Considering both the model agreement and strong anthropogenic signal, the precipitation trends in the deep tropics should be relatively certain. Therefore, it is reasonable to use this domain to evaluate how well the AR1 model estimates the spread of the CCSM model.

Output from the CCSM model reveals that the deep tropics receive a higher amount of annual precipitation than other regions around the globe (Figure 5.5). Also, the model predicts that the deep tropics will experience the largest increase in rainfall over the next 50 years. The left panel of Figure 5.8 shows the time series of all CCSM realizations. In this figure, all trends are positive, which indicates that the amount of precipitation in the deep tropics will likely increase.

The right panel of Figure 5.8 illustrates how the CCSM and AR1 model share the same amount spread. Here, the mean of the trends from the CCSM model is 0.035 mm/m2/decade, with a spread of 2.5e-3 0.035 mm/m2/decade. Similarly, the AR1 model has a mean trend of 0.036 0.035 mm/m2/decade and a spread of 2.9e-3 0.035 mm/m2/decade. From these results, it is assumed that the AR1 model captures the spread of the CCSM model.

The right panel of Figure 5.8 suggests that all of the precipitation trends in both the CCSM and AR1 model are positive and significant. If the ensemble mean of the model is

indicative of the future climate, then it is virtually certain that the trend in precipitation in the deep tropics will be statistically significant from zero. As a result, it should be possible to extract the anthropogenic signal from the precipitation field within the deep tropics over the next 50 years.

4.4 Circulation

As stated previously, some components of the atmospheric circulation may undergo significant changes in response to increasing greenhouse gases. The changes in the atmospheric circulation can drive changes in other components within the atmosphere. In this study, we use the CCSM and AR1 model to assess how various components of the atmospheric circulation will change in response to the anthropogenic forcing.

Although there are many measures and components of the atmospheric circulation, this study will limit the circulation to the annular modes, jet latitude, and width of the tropics. When possible, the circulation will be assessed in both the Northern and Southern Hemispheres. For completeness, the circulation will be viewed seasonally (DJF and JJA) and annually.

4.4.1. Annular Modes

The annular modes are dipole patterns of anomalous high and low pressure over the poles and midlatitudes. The positive [negative] phase of the annular modes is marked by an anomalously low [high] pressure over the pole and anomalously high [low] pressure in the midlatitudes. Because the annular modes are strongly tied to the atmospheric circulation, the phase of the annular mode can influence the position of the jet, Hadley Cell, and storm tracks.

4.4.1.1 Northern Hemisphere Annular Mode

The NAM index is derived by standardizing the first principal component from the 20˚N-90˚N sea level pressure field. The CCSM and AR1 NAM index results are shown in Figure 5.9. Here, the left column shows the CCSM NAM index time series from 2000-2060, with the ensemble mean in black. From top to bottom, the rows show the results for the annual mean, the DJF seasonal mean, and the JJA seasonal mean NAM index. The right column of the figure shows the distribution of the CCSM NAM trends and the AR1 fit. Overall, the CCSM model suggests that the annual mean NAM index should exhibit a positive trend over the first half of the 21st century. This is due to the fact the CCSM and AR1 ensembles share a mean trend of 0.028 std/decade. Seasonally, the CCSM and AR1 ensemble mean is positive during the boreal winter and summer months. Since the ensemble mean is positive in both winter and summer, it further implies that NAM is more likely to trend towards its positive phase over the next 50 years.

When comparing the AR1 and CCSM model, the AR1 model reproduces the CCSM model spread across all time domains studied. Annually, the CCSM and AR1 model generate a spread of 0.028 mb/decade. For the boreal winter, the AR1 model replicates 90% of the CCSM spread. However the AR1 model replicates 98% of the CCSM spread during the boreal summer. The results indicate that the AR1 model performs better during JJA, when the amplitude of the variability is smaller.

In regards to the significance of the trends, the CCSM and AR1 ensemble mean trend is statistically significant annually and for both seasons studied. However, the CCSM model estimates that 15% of the individual annual mean NAM index trends in the model will be significant, and only 8% and 5% of the boreal winter and summer trends will be significant. As

expected, the AR1 model behaves like the CCSM model and gives similar estimates on the percent of significant members.

4.4.1.2 Southern Hemisphere Annular Mode

Although the NAM and SAM are similar patterns of variability, the SAM's trend behaves differently because of ozone recovery in the Southern Hemisphere. One aspect that distinguishes the NAM from the SAM is that the SAM trends show more seasonality than the NAM [*Gillett and Fyfe,* 2013]. This is shown in Figure 5.10. Annually, the ensemble mean SAM trend is positive in both the CCSM and AR1 model. When assessed seasonally, the ensemble mean of the two models is positive during the austral winter, and negative during the austral summer. Since the annual SAM trend is positive, it is likely that the annual mean trend of the SAM index is mostly dominated by the months JJA, rather than DJF. With these results, it is important to note that the CCSM model does include ozone depletion.

In terms of significance, the models produce a significant ensemble mean for the annual SAM index. This suggests that it is more likely for the SAM to shift to its positive phase. However, the real climate will behave like an individual realization, which has roughly a 10% chance of being significant. Therefore, the significance of the SAM trend from 2000-2060 will depend heavily on the natural variability. Beyond 2060, the SAM trend should become more clear, since it is likely that the ozone hole will recover by then.

4.5 Jet latitude

The jet latitude is defined as the latitude that corresponds to the strongest westerly zonal mean zonal wind at 850mb. The native resolution from the CCSM model is 2.5˚x 2.5˚, but the

shift in the jet latitude is likely to be much smaller than 2.5˚. This means that the jet latitude is not resolved in the CCSM model. Also, the jet can only shift in discrete increments. As a means of circumventing this issue, the data from the CCSM model was interpolated to a grid that is approximately 0.63˚ x 0.63˚ in resolution.

4.5.1 Northern Hemisphere Jet

The long-term mean position of the jet in the CCSM model is roughly 45 degrees latitude. However, the jet shifts equatorward during the winter months and shifts poleward during the summer months. Despite the seasonal shifts of the jet, climate change can alter the seasonal and annual mean position of the jet. Previous studies have concluded that the jet should shift poleward in response to an anthropogenic forcing [*Barnes and Polvani,* 2013].

Figure 5.11 is the same as Figures 5.9 and 5.10, except the figure shows the predicted behavior of the jet instead of the annular modes over the next 50 years. The left columns show the annual and seasonal time series that are produced by the CCSM ensemble. The right columns show that mean trend of the jet is 0.13, 0.10, and 0.16 degrees-poleward/decade for the annual, DJF, and JJA mean respectively. The trends in the jet latitudes are consistent with the trends in the annular modes, in the sense that the ensemble mean is positive. Additionally, the likelihood of the real climate exhibiting a significant shift in the jet is very small.

4.5.2 Southern Hemisphere Jet

The jet in the Southern Hemisphere behaves in a similar manner to the Northern Hemisphere jet. The key difference in the basic state between the two jets is that the mean position of the Southern Hemisphere jet is poleward relative to the Northern Hemisphere jet

(Figure 5.12 left panel). Despite the differences in the jet positions, they appear to agree on the sign of the trends for all time domains. Like the Northern Hemisphere, the AR1 model is equally valid at estimating the spread of the CCSM jet latitude. The Southern Hemisphere jet generally agrees and correlates with the SAM index. Specifically, the jet shows the same seasonality as the SAM. However, there is less correlation when the jet trend is viewed annually. Additionally, the probability of a significant shift in the jet's latitude is low, which means that it is unlikely that we will detect a jet shift in the future.

4.6 Tropic Width

The response of the Hadley Cell or width of the tropics to an anthropogenic forcing is not well understood. The tropics are expected to expand and weaken, in response to an anthropogenic forcing, but the amount is still uncertain [*Vecchi and Soden* 2007; *Son et al.,* 2009]. Difficulty in estimating the expansion of the tropics lies within our understanding of dynamics and our ability resolve such an expansion. Furthermore, the expansion of the tropics varies depending on the definition of the tropics.

For this study, the edges of the tropics are defined where the 850mb wind goes to zero. This boundary clearly marks the westerlies in the mid-latitudes and the easterlies in the tropics. The winds at 850mb were chosen because it is the top of the boundary layer and it serves as a good diagnostic of where the jet imparts westerly momentum to the lower levels of the atmosphere. As in the jet latitude assessment, the CCSM model was interpolated from 2.5˚X2.5˚ to a resolution of 0.63˚X 0.63˚.

Figure 5.13 shows the results of the width of the tropics. The left column of the figure shows the CCSM time series of the width of the tropics for different seasons. The right column

of the figure shows the histogram and significance of the CCSM and AR1 trends. Overall, the figure suggests that it is more likely than not that the tropics will expand in response to climate change. However, the models suggest that there is roughly a one in four chance that the annual trend in the tropic width will be significant.

Additionally, the trends in the width of the tropics show little seasonality. The figure reveals that the annual, DJF, and JJA mean width of the tropics is 0.05, 0.05, and 0.07 degrees per decade. Not only are the trends consistent across seasons, but the significance is consistent as well. Across all seasons, the CCSM and AR1 models suggest that there is a 0-6% chance that the tropics will widen significantly over the next 50 years.

4.7 Summary

The results of this work agree with prior studies such as *Deser et al.* 2012 and *Hawkins and Sutton* 2010. Like the prior studies, this work has shown that the internal variability within the climate system adds to the uncertainty in climate projections. Because of the uncertainty, it is difficult to make accurate projections of the future climate.

In this chapter, we quantified the spread of the 40-member ensemble climate trends, so that we can understand how uncertain various climate trends are. The figures in the chapter serve as a visual reference of how uncertain climate trends are, and they allow one to see the range of possible climate outcomes. In addition, we use the spread in the 40-member ensemble trends to make probabilistic forecasts on significant climate change. The results of this work emphasize the importance of estimating the significance of an individual realization of the climate, instead of the ensemble mean trend. This is because the ensemble mean time series filters out *climate noise* that exits in the real world, which means the real climate will behave like an ensemble

member, rather than the ensemble mean. Finally, the results of this chapter highlight the fact that detecting a significant change in some aspects of the climate may depend on the behavior of the natural internal variability.

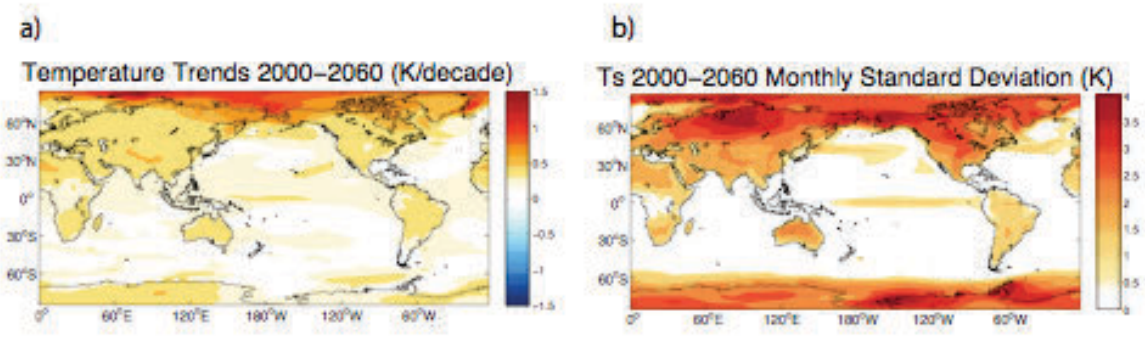

Figure 4.1 a) Shows the ensemble mean DJF surface temperature trends for the CCSM model. b) Shows the standard deviation of the detrended monthly surface temperature from 2000-2060 in an arbitrary CCSM model realization

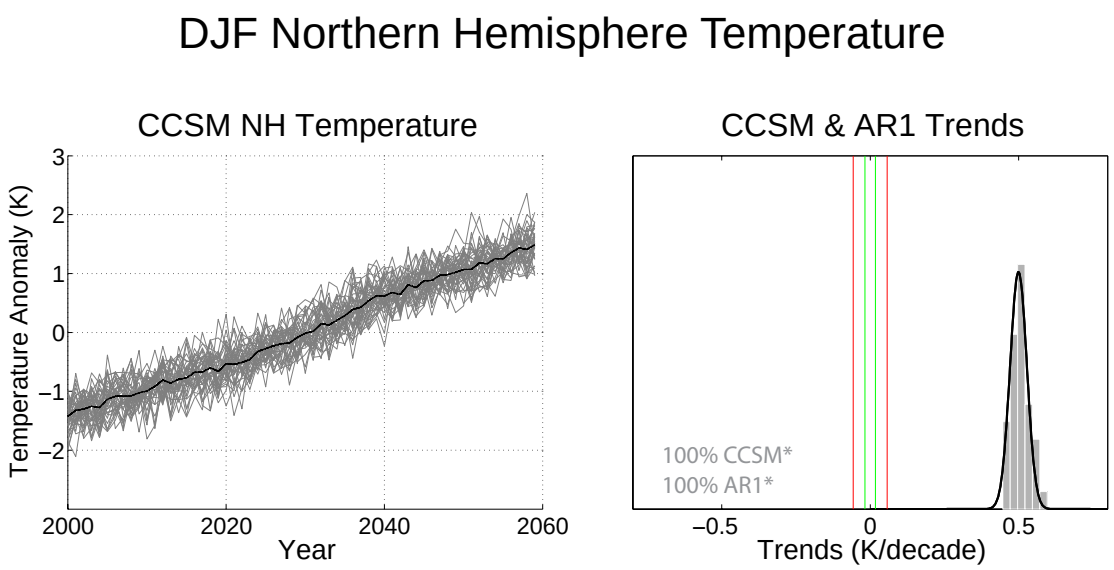

Figure 4.2 The left panel shows all 40 Northern Hemisphere DJF surface temperature time series produced by the CCSM model. The black curve represents the ensemble mean of the output. The right panel shows a histogram of the surface temperature trends of the CCSM model (gray bars). The black curve is the normal fit for the 1000-member AR1 ensemble. The red line represents the significance threshold for an ensemble member, and the green line is the significance threshold for the ensemble mean. The percent in the lower left represent the percent of the CCSM and AR1 members that are significant. The asterisks indicate if the ensemble mean is significant.

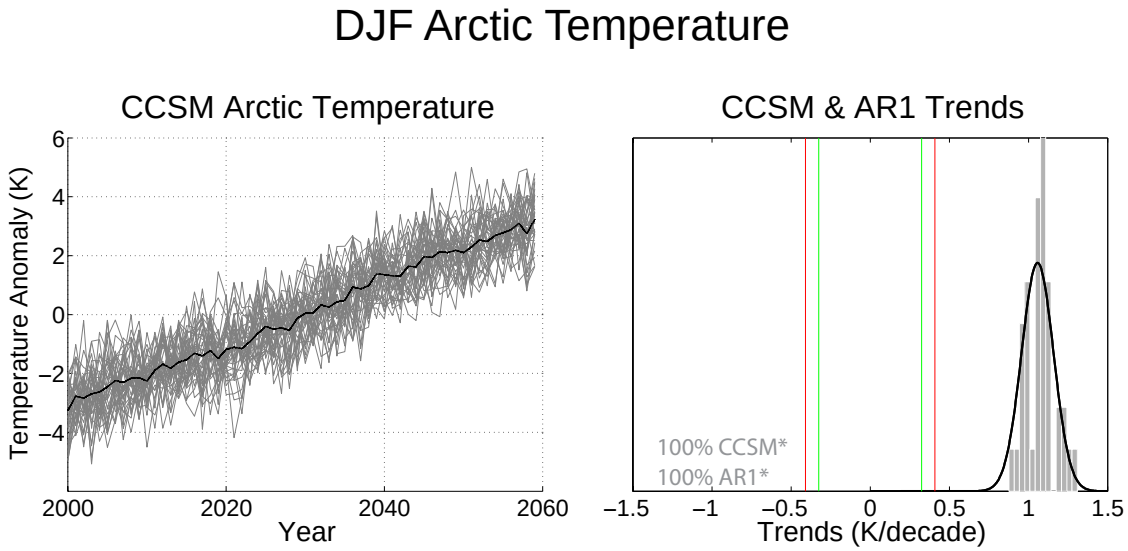

Figure 4.3 Same as Figure 4.2 but for the Arctic

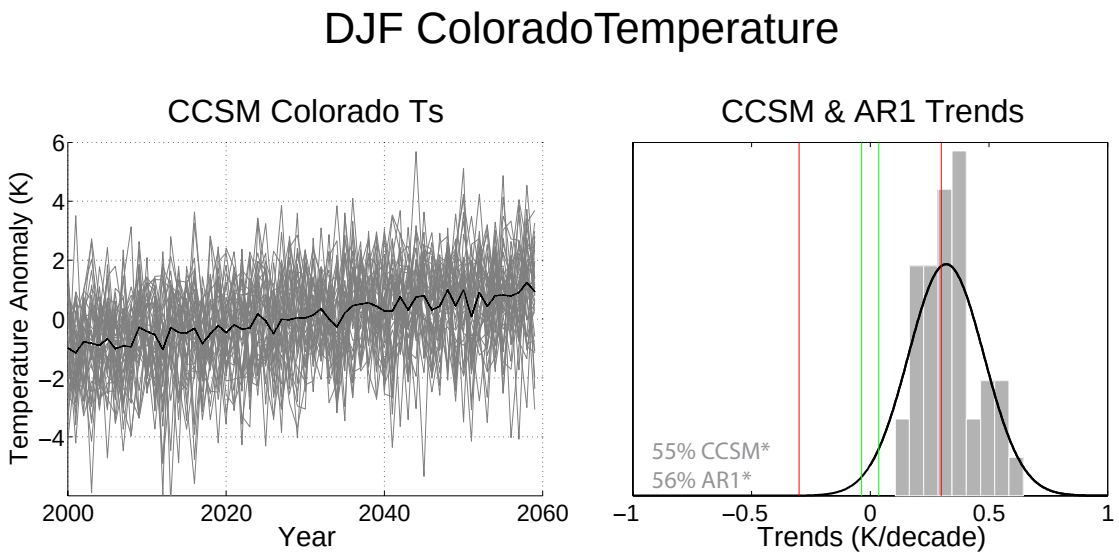

Figure 4.4 Same as Figure 4.2 but for Colorado

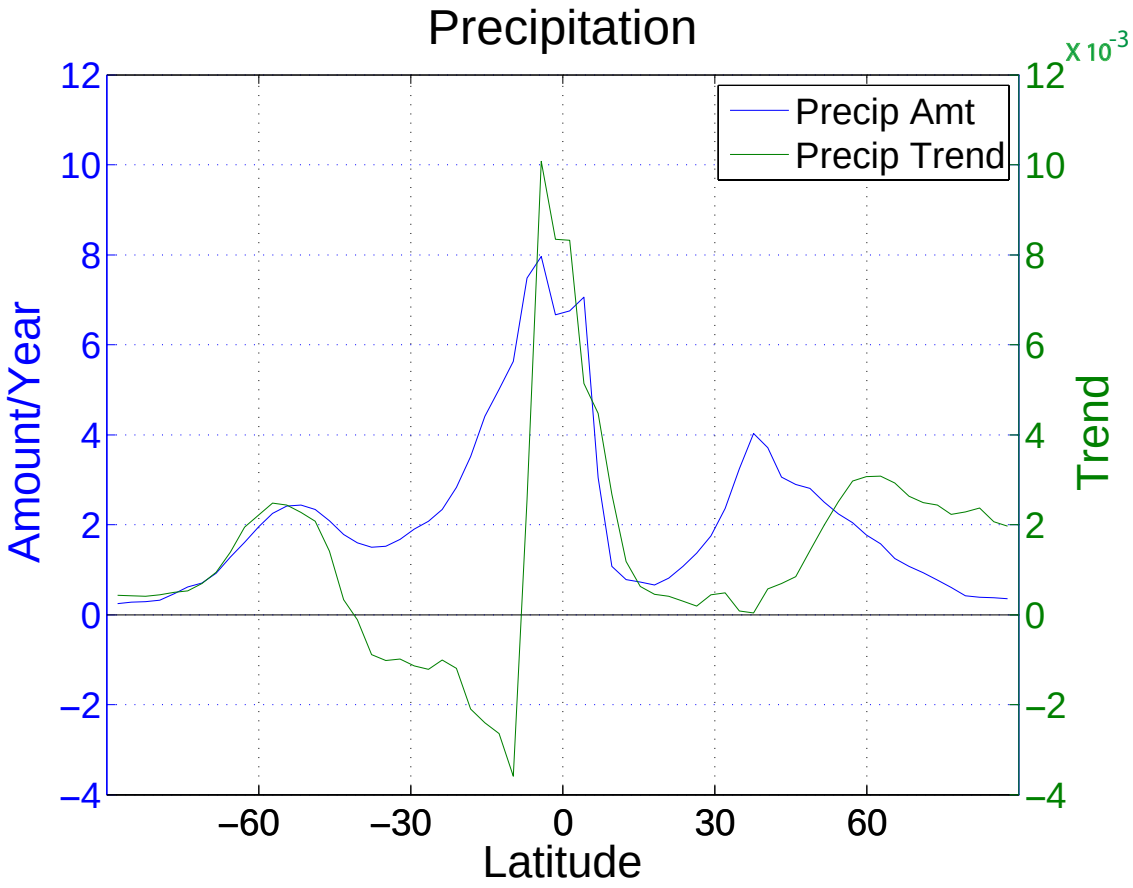

Figure 4.5 The blue curve represents the CCSM ensemble mean zonal mean precipitation rate in mm/m2/day. The green curve shows the trend in the amount of precipitation per decade from 2000-2060

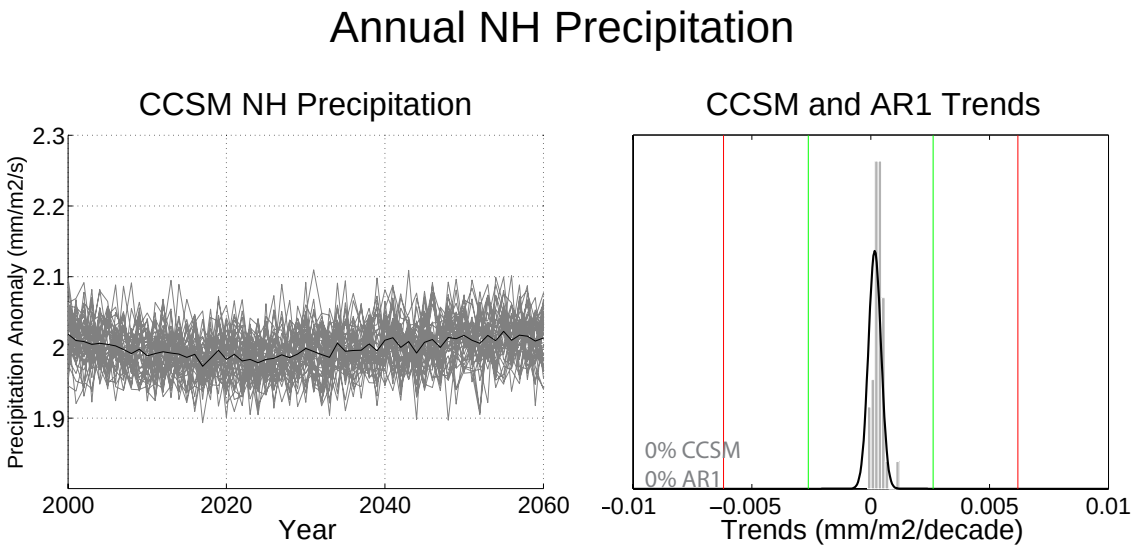

Figure 4.6 The left panel shows all 40 Northern Hemisphere annual precipitation anomaly (mm/m2/day) time series produced by the CCSM model. The black curve represents the ensemble mean of the output. The right panel shows a histogram of the precipitation trends (mm/m2/decade) of the CCSM model (gray bars). The black curve is the normal fit for the 1000-member AR1 ensemble. The red line represents the significance threshold of an ensemble member, and the green line is the threshold for significance for the ensemble mean. The percents in the lower left represent the percent of CCSM and AR1 member that are significant. The asterisks indicate if the ensemble mean is significant.

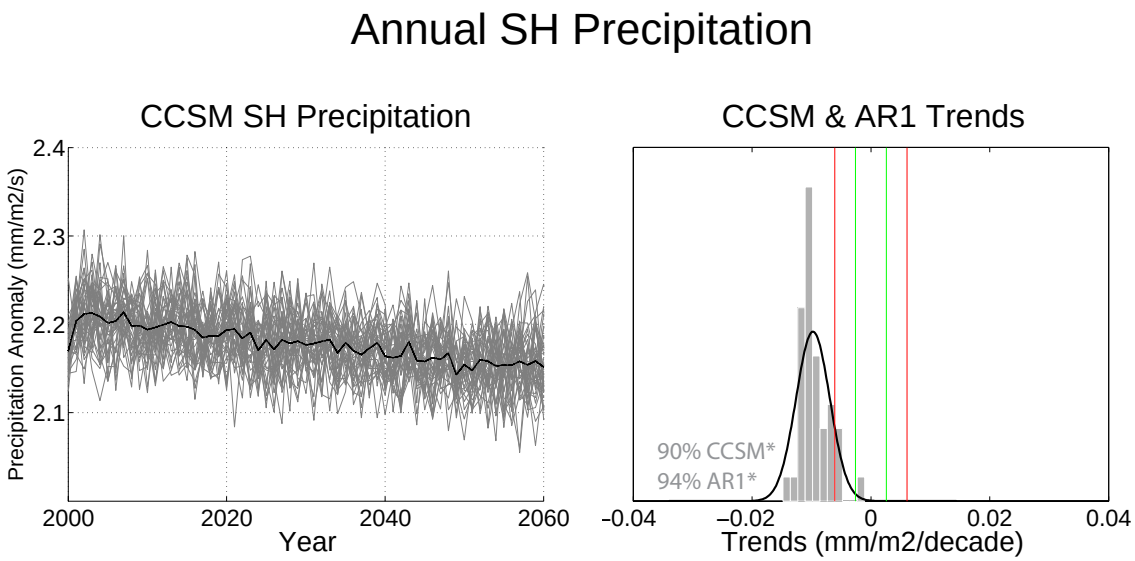

Figure 4.7 Same as Figure 4.6 but for annual precipitation in the Southern Hemisphere (15S-40S)

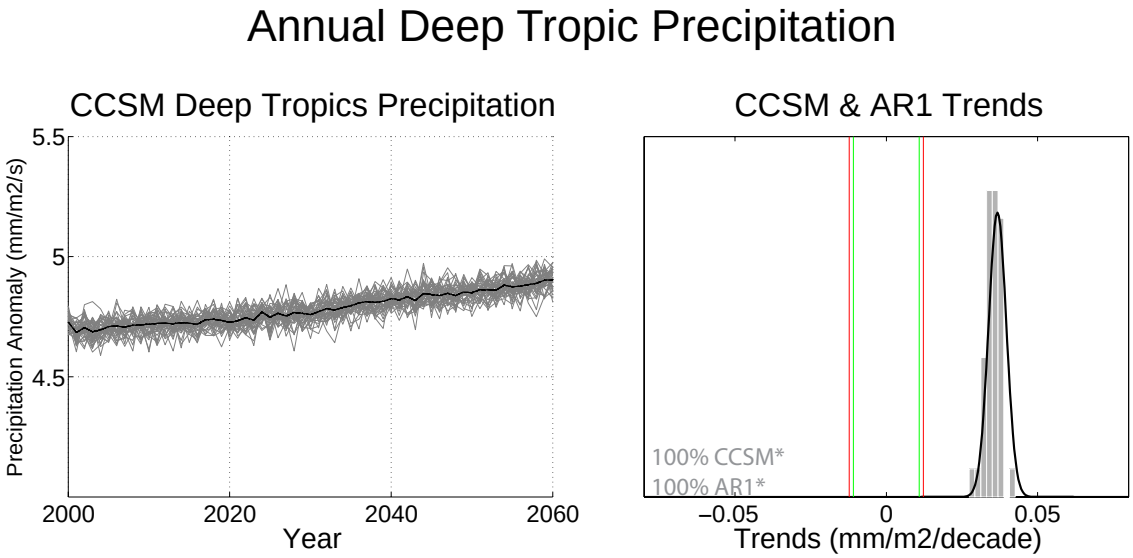

Figure 4.8 Same as Figure 4.6 but for annual precipitation in the Deep Tropics (15N-15S)

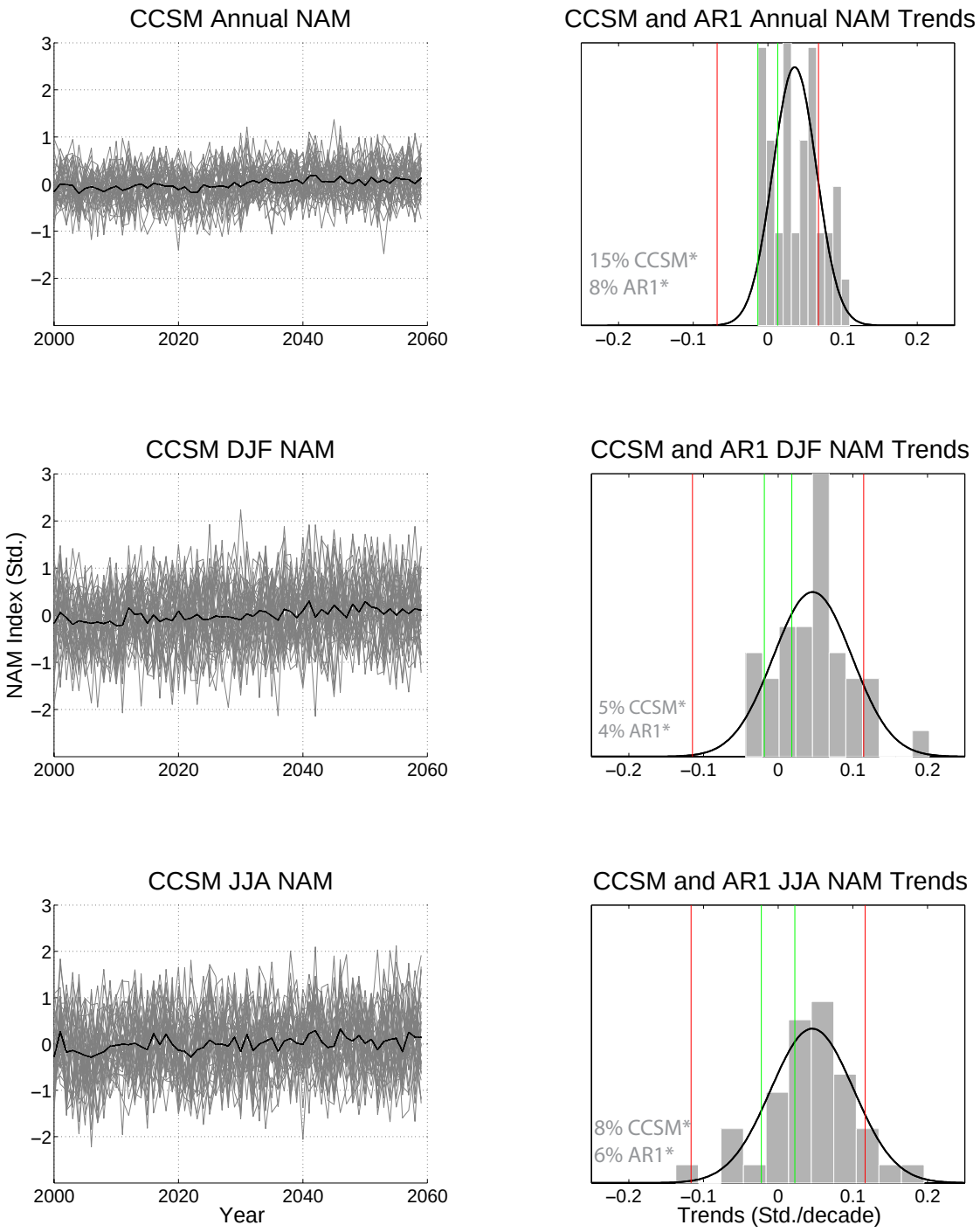

Figure 4.9 The left column shows all 40 Northern Hemisphere Annual, DJF, and JJA NAM index (units of standard deviations of sea level pressure) time series produced by the CCSM model. The black curve represents the ensemble mean of the output. The right column shows histograms of the NAM trend (std./decade) of the CCSM model (gray bars). The black curve is the normal fit for the 1000-member AR1 ensemble. The red line represents the threshold for significance for an ensemble member, and the green line is the threshold for significance for the ensemble mean. The percents listed in the lower left of the figures represent the percentage of CCSM and AR1 members that are statistically significant from zero.

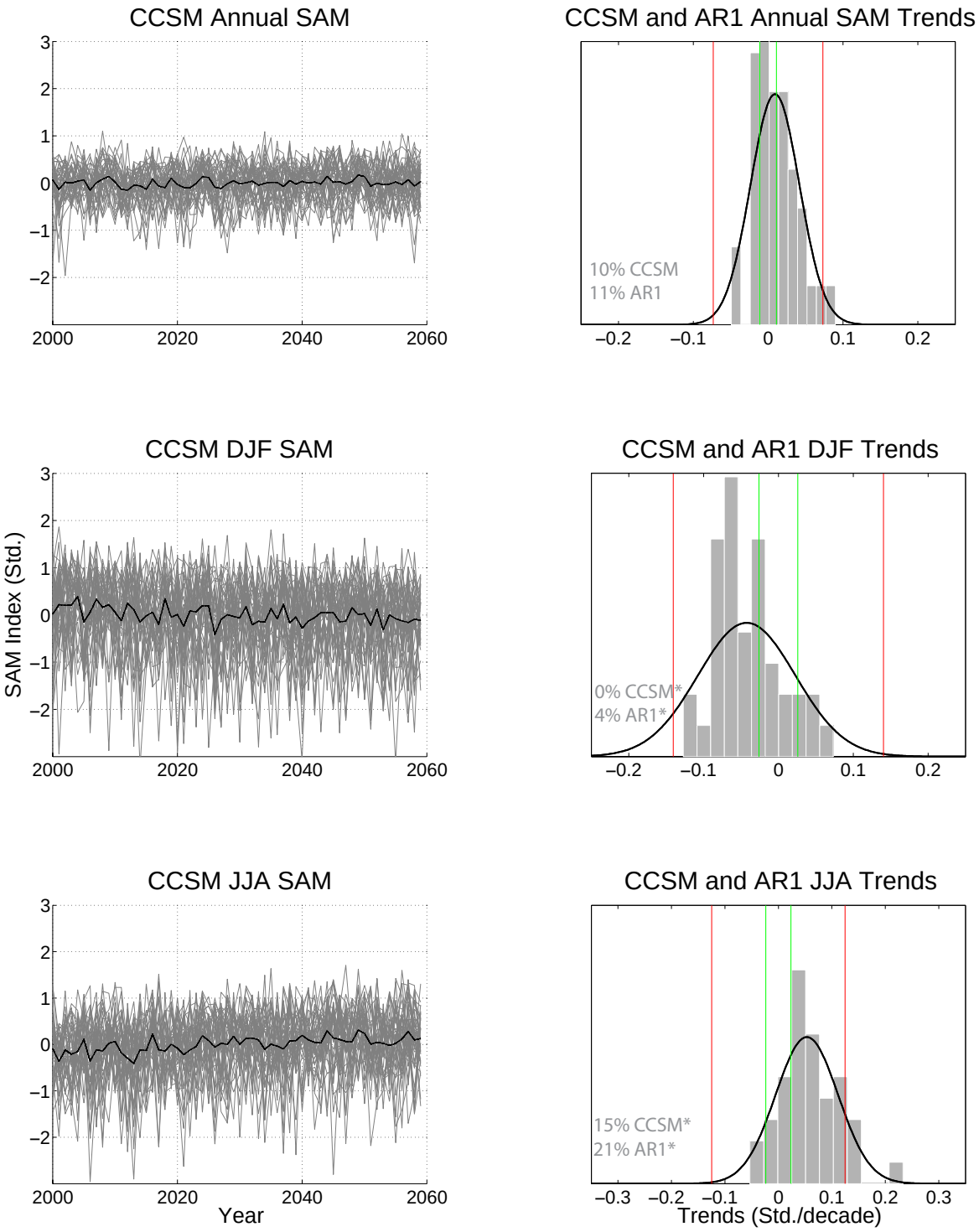

Figure 4.10 Same as Figure 4.9 but for the JJA SAM index.

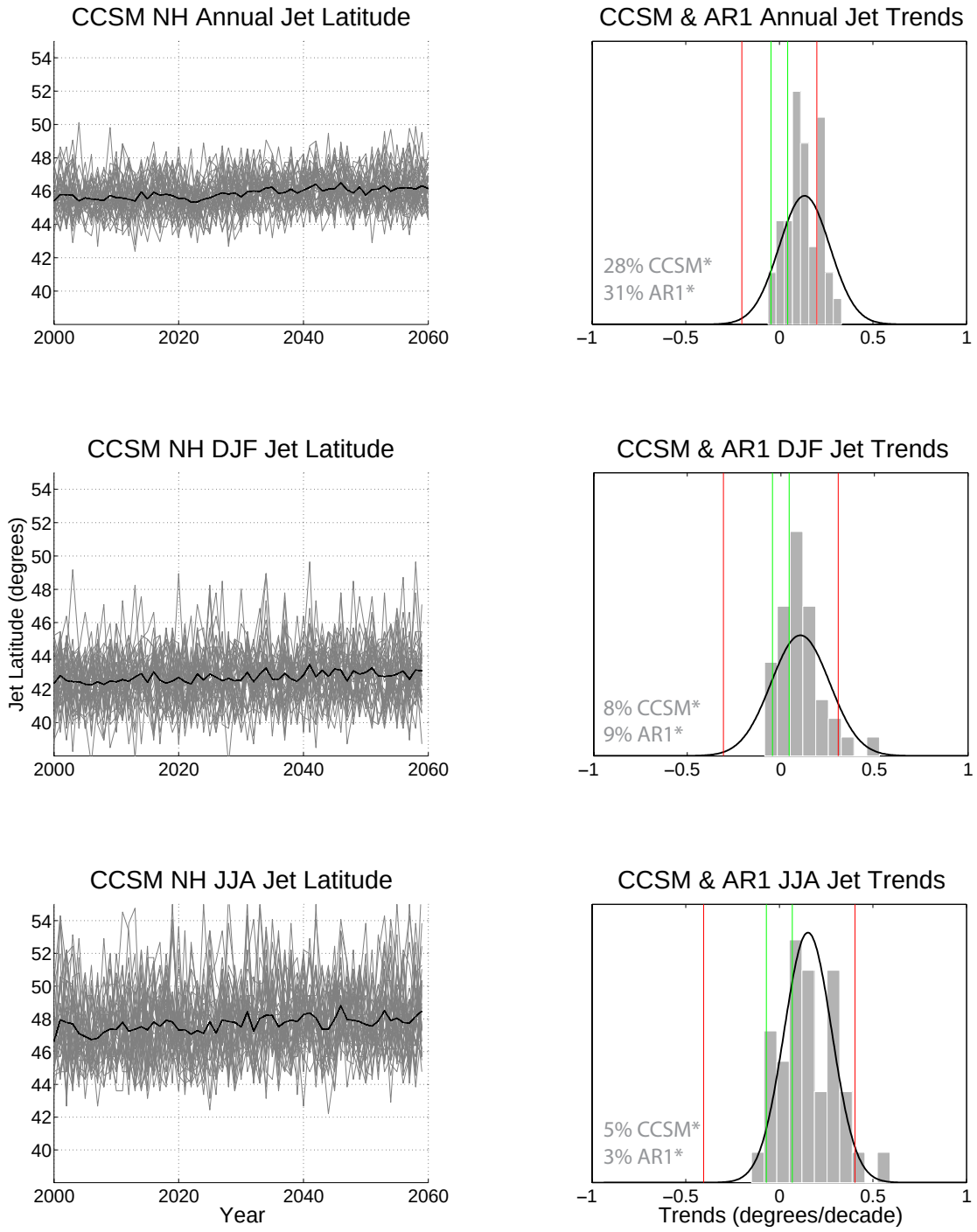

Figure 4.11 The left column shows all 50 jet latitude time series produced by the CCSM model. The black curve represents the ensemble mean of the output. The right column shows a histogram of the NAM trends (degrees/decade) of the CCSM model (gray bars). The black curve is the normal fit for the 1000-member AR1 ensemble. The red line represents the significance threshold for an ensemble member, and the green line is the significance threshold for the ensemble mean. The percents in the lower left corner of the figures represent the percentage of CCSM members that are significant relative to the ensemble mean. The asterisks indicate the significance of the ensemble mean.

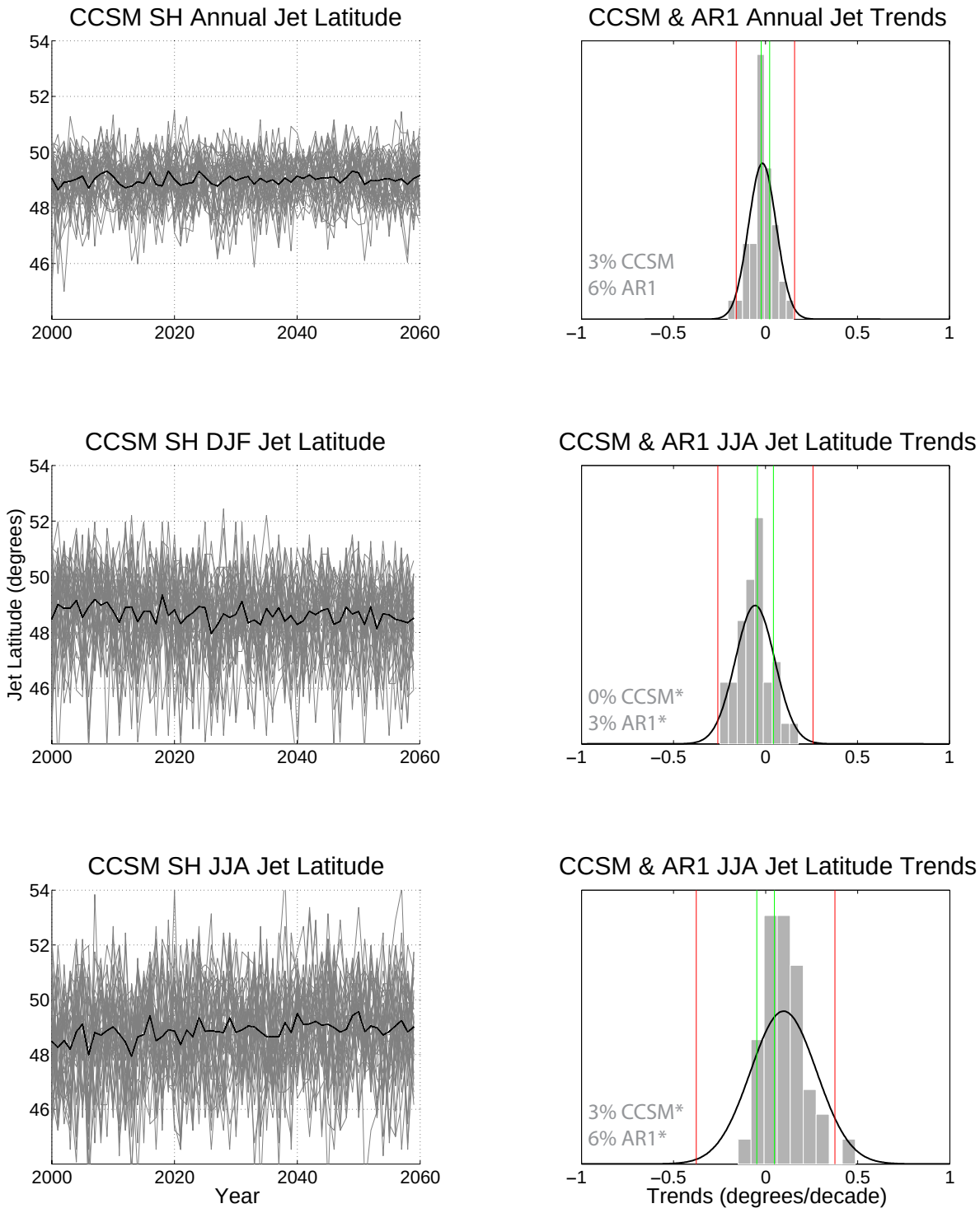

Figure 4.12 Same as Figure 4.11 but for the Southern Hemisphere JJA jet latitudes. Data is oriented such that higher values represent a poleward position of the jet

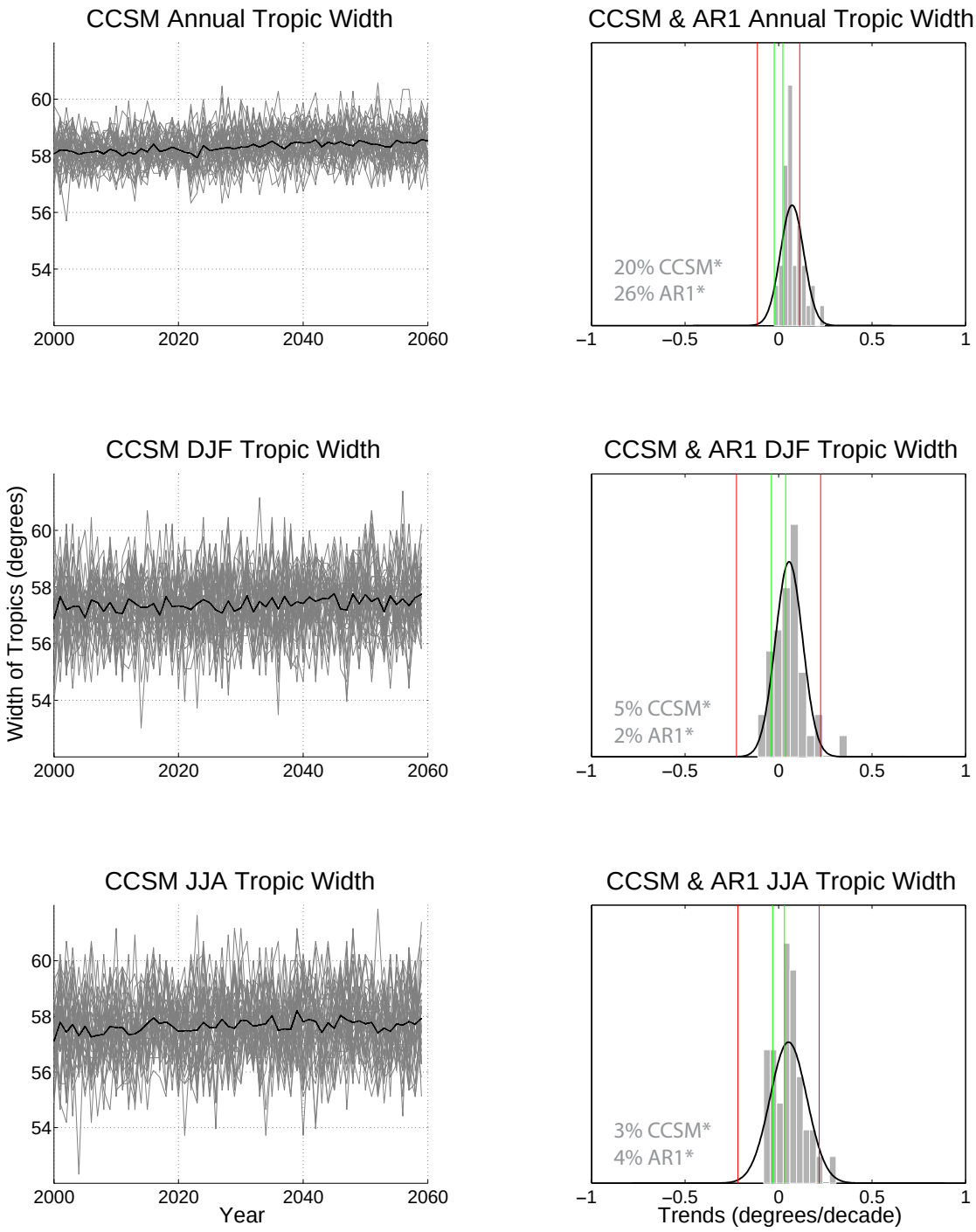

Figure 4.13 The left column of panels shows all 40 tropic width time series produced by the CCSM model for all time domains. The black curve represents the ensemble mean of the output. The right panel shows a histogram of the tropic width trends (degrees/decade) of the CCSM model (gray bars). The black curve is the normal fit for the 1000-member AR1 ensemble. The red line represents the significance threshold for an ensemble member, and the green line is the significance threshold for the ensemble mean. The percents indicate the number of CCSM and AR1 members that are significant. The asterisks indicate the significance of the ensemble mean.

Chapter 5

Conclusion

5.1 Summary

Prior studies show that the amplitude of the internal variability is larger on local spatial scales, which makes trends less certain [Hawkins and Sutton 2010; Deser et al. 2012]. As a result, it is difficult to estimate the probability that trends will be significant on local spatial scales, or estimate the significance of variables that contain a high amount of month-to-month variability. Previous work attempted to assess the internal variability and make probabilistic forecasts, but the results could be improved with more ensemble members.

In this study, we used the NCAR 40-member ensemble and an AR1 model to estimate the uncertainty due to internal variability and the likelihood of future climate trends being significant. The AR1 model supplements the realizations of the 40-member ensemble by producing an analytic solution for the distribution of an infinite number of realizations. With the 40-member ensemble and the AR1 model, we are able to more accurately assess the significance of climate trends.

The AR1 model was chosen to supplement the 40-member ensemble realizations because the AR1 model outperformed both of the circulation models by capturing more of the spread in trends from the 40-member ensemble. Since the AR1 model performed better than the circulation models, it implies that the month-to-month variability in the atmospheric circulation alone cannot fully explain the variance in the surface temperature field. In lieu of this finding, it is likely that the circulation will not be able to fully explain the variance in other state variables of the climate.

The result of this study determines that that the significance of large-scale surface temperature trends is unanimous, such that all realization of the NCAR and AR1 model are significant. Both of the model show a high probability that the Northern Hemisphere and Arctic mean surface temperature trends will also be significant. However, this study highlighted that local and regional surface temperature trends are less certain. Particularly on local spatial scales, it is important to determine the probability that a single realization is significant rather than the ensemble mean.

The certainty of the trends in the precipitation field was shown to vary regionally. The zonal mean precipitation field in the deep tropics shows a robust response to the anthropogenic forcing. Under the assumption that the NCAR model represents the future climate well, it is virtually assured that the zonal mean precipitation in the deep tropics will increase significantly, because all members of the NCAR and AR1 model are significant. The precipitation field in the Southern Hemisphere subtropics was shown to be the most, because the ensemble spread is largest here, and models estimate that there is roughly a 90% chance that a realization will be significant. The ensemble mean of the subtropical Southern Hemisphere mean precipitation field indicates that precipitation is more likely to decrease, but the internal variability makes this difficult to assess. Generally, changes to the atmospheric circulation are uncertain. The uncertainty spans the annular modes, jet latitude, and width of the tropics. As a result, it may be difficult to observe the effects of climate change on the atmospheric circulation.

This study has shown multiple scenarios where the ensemble mean is significant, and many ensemble members are insignificant. Under these circumstances, the significance of the climate trend depends on how the internal variability affects the magnitude of the trend. This outcome stresses the importance of assessing the significance of individual realizations as

opposed to the ensemble mean. As shown in previous sections of the text, the ensemble mean can sometimes be misleading if it is shrouded in large amplitudes of internal variability.

5.2 Future Work

As shown in *Hawkin and Sutton* [2009], the internal variability causes most of the uncertainty in near-term local climate forecasts. The methods used in this study can serve as a tool to improve near-term probabilistic climate forecasts, by using an ensemble and an AR1 model to estimate the spread and likelihood of significant climate trends. Additionally, this work can be adopted to make probabilistic forecasts for other atmospheric variables and other regions of the globe.

Since the NCAR 40-member ensemble was used, this study only assesses how the internal variability affects the trends. The methods used can be applied to other perturbed initial condition ensembles, or to perturbed physics ensembles and perturbed forcing ensembles. Appling these methods to a perturbed physics or forcing ensemble will allow one to evaluate the effects of model physics or an anthropogenic forcing on climate predictions. Lastly, this work analyzed a small quantity of climate variables, but it can be applied to nearly any aspect of the climate. A more comprehensive analysis may provide clues as to whether certain aspects of the climate system are more sensitive to an anthropogenic forcing or the internal variability.

References

Allen, M. R., and L. A. Smith, 1994: Investigation the origins and significance of low-frequency modes of climate variability. *Geophys. Res. Lett.*, **21**, 883–886.

Arblaster, J. M., and G. a. Meehl, 2006: Contributions of External Forcings to Southern Annular Mode Trends. *J. Clim.*, **19**, 2896–2905, doi:10.1175/JCLI3774.1.

Bailey, D. H., R. Barrio, and J. M. Borwein (2012), High-precision computation: Mathematical physics and dynamics, *Appl. Math. Comput.*, *218*(20), 10106–10121, doi:10.1016/j.amc.2012.03.087.

Barnes, E. a., and L. Polvani, 2013: Response of the Midlatitude Jets, and of Their Variability, to Increased Greenhouse Gases in the CMIP5 Models. *J. Clim.*, **26**, 7117–7135, doi:10.1175/JCLI-D-12-00536.1.

Ceppi, P., and D. L. Hartmann, 2013: On the Speed of the Eddy-Driven Jet and the Width of the Paulo Ceppi. *J. Clim.*, **26**, 3450–3465, doi:10.1175/JCLI-D-12-00414.1.

Daithi, A. S., and J. W. Andrew, 2001: Projection of Climate Change onto Modes of Atmospheric Variability. *J. Clim.*, **14**, 3551–3565.

Deser, C., A. S. Phillips, M. a. Alexander, and B. V. Smoliak, 2014: Projecting North American Climate over the Next 50 Years: Uncertainty due to Internal Variability*. *J. Clim.*, **27**, 2271–2296, doi:10.1175/JCLI-D-13-00451.1.

Deser, C., A. Phillips, V. Bourdette, and H. Teng, 2010: Uncertainty in climate change projections: the role of internal variability. *Clim. Dyn.*, **38**, 527–546, doi:10.1007/s00382-010-0977-x.

Deser, C., R. Knutti, S. Solomon, and A. S. Phillips, 2012: Communication of the role of natural variability in North American climate. *Nat. Clim. Chang.*, **2**, 775–779, doi:10.1038/NCLIMATE1562.

Frierson, D. M. W., J. Lu, and G. Chen, 2007: Width of the Hadley cell in simple and comprehensive general circulation models. *Geophys. Res. Lett.*, **34**, doi:10.1029/2007GL031115.

Gillett, N. P., and J. C. Fyfe, 2013: Annular mode changes in the CMIP5 simulations. *Geophys. Res. Lett.*, **40**, 1189–1193, doi:10.1002/grl.50249.

Hawkins, E., and R. Sutton, 2009: The Potential to Narrow Uncertainty in Regional Climate Predictions. *Bull. Am. Meteorol. Soc.*, **90**, 1095–1107, doi:10.1175/2009BAMS2607.1.

Hawkins, E., and R. Sutton, 2010: The potential to narrow uncertainty in projections of regional precipitation change. *Clim. Dyn.*, **37**, 407–418, doi:10.1007/s00382-010- 0810-6.

Held, I. M., and B. J. Soden, 2006: Robust Responses of the Hydrological Cycle to Global Warming. *J. Clim.*, **19**, 5686–5699.

Collins, W. D. et al. (2006), The Community Climate System Model Version 3 (CCSM3), *J. Clim.*, *19*(11), 2122–2143.

Huntingford, C., P. D. Jones, V. N. Livina, T. M. Lenton, and P. M. Cox, 2013: No increase in global temperature variability despite changing regional patterns. *Nature*, **500**, 327–330, doi:10.1038/nature12310.

IPCC, 2007: Climate Change 2007: The Physical Science Basis. Contribution of Working Group I to the Fourth Assessment Report of the Intergovernmental Panel on Climate Change [Solomon, S., D. Qin, M. Manning, Z. Chen, M. Marquis, K.B. Averyt, M.Tignor and H.L. Miller (eds.)]. Cambridge University Press, Cambridge, United Kingdom and New York, NY, USA.

Kang, S. M., C. Deser, and L. M. Polvani, 2013: Uncertainty in climate change projections of the Hadley circulation: the role of internal variability. *J. Clim.*, **26**, 7541–7554, doi:10.1175/JCLI-D-12-00788.1.

Kidston, J., C. Cairns, and P. Paga, 2013: Variability in the width of the tropics and the annular modes. *Geophys. Res. Lett.*, **40**, 2328–2332, doi:10.1029/2012GL054165.

Knutti, R., R. Furrer, C. Tebaldi, J. Cermak, and G. a. Meehl, 2010: Challenges in Combining Projections from Multiple Climate Models. *J. Clim.*, **23**, 2739–2758, doi:10.1175/2009JCLI3361.1.

Knutti, R., and J. Sedláček, 2012: Robustness and uncertainties in the new CMIP5 climate model projections. *Nat. Clim. Chang.*, **3**, 369–373, doi:10.1038/nclimate1716.

Lorenz, E. N., 1963: Deterministic Nonperiodic Flow. *J. Clim.*, **20**, 130–141, doi:dx.doi.org/10.1175/1520- 0469(1963)020<0130:DNF>2.0.CO;2.

Lu, J., G. a. Vecchi, and T. Reichler, 2007: Expansion of the Hadley cell under global warming. *Geophys. Res. Lett.*, **34**, 2–6, doi:10.1029/2006GL028443.

Madden, R. A., 1976: Estimates of the Natural Variability of Time-Averaged Sea-Level Pressure. *Mon. Weather Rev.*, **104**, 942–952, doi:dx.doi.org/10.1175/1520 0493(1976)104<0942:EOTNVO>2.0.CO;2.

Miller, R. L., G. a. Schmidt, and D. T. Shindell, 2006: Forced annular variations in the 20th century Intergovernmental Panel on Climate Change Fourth Assessment Report models. *J. Geophys. Res.*, **111**, D18101, doi:10.1029/2005JD006323.

Morgan, G., H. Dowlatabadi, M. Henrion, D. Keith, R. Lempert, S. McBride, M. Small, and T. Wilbanks, 2009: *Best Practice Approaches for Communicating , and Incorporating Scientific Uncertainty in Climate Decision Making*. Washington, DC,.

Nakićenović, N., and Swart, R. (2000), *Special Report on Emissions Scenarios: A special report of Working Group III of the Intergovernmental Panel on Climate Change*, Cambridge University Press,

Pielke, R. A., R. Avissar, M. Raupach, A. J. Dolman, X. Zeng, and A. S. Denning, 1998: Interactions between the atmosphere and terrestrial ecosystems: influence on weather and climate. *Glob. Chang. Biol.*, **4**, 461–475, doi:10.1046/j.1365-2486.1998.t01-1-00176.x.

Polade, S. D., D. W. Pierce, D. R. Cayan, A. Gershunov, and M. D. Dettinger, 2014: The key role of dry days in changing regional climate and precipitation regimes. *Sci. Rep.*, **4**, 4364, doi:10.1038/srep04364.

Polvani, L. M., M. Previdi, and C. Deser, 2011: Large cancellation, due to ozone recovery, of future Southern Hemisphere atmospheric circulation trends. *Geophys. Res. Lett.*, **38**, L04707, doi:10.1029/2011GL046712

Quadrelli, R., and J. M. Wallace, 2004: A Simplified Linear Framework for Interpreting Patterns of Northern Hemisphere Wintertime Climate Variability. **17**, 3728–3744.

Sanderson, B. M., C. Piani, W. J. Ingram, D. a. Stone, and M. R. Allen, 2007: Towards constraining climate sensitivity by linear analysis of feedback patterns in thousands of perturbed-physics GCM simulations. *Clim. Dyn.*, **30**, 175–190, doi:10.1007/s00382-007-0280-7.

Santer, B. D., T. M. L. Wigley, J. S. Boyle, D. J. Gaffen, J. J. Hnilo, D. Nychka, D. E. Parker, and K. E. Taylor, 2000: Statistical significance of trends and trend differences in layer-average atmospheric temperature time series. *J. Geophys. Res.*, **105**, 7337–7356, doi:10.102.

Santer, B. D., and Coauthors, 2011: Separating signal and noise in atmospheric temperature changes: The importance of timescale. *J. Geophys. Res.*, **116**, doi:10.1029/2011JD016263.

Seidel, D. J., Q. Fu, W. J. Randel, and T. J. Reichler, 2008: Widening of the tropical belt in a changing climate. *Nat. Geosci.*, **1**, 21–24, doi:10.1038/ngeo.2007.38.

Serreze, M. C., A. P. Barrett, and J. J. Cassano, 2011: Circulation and surface controls on the lower tropospheric air temperature field of the Arctic. *J. Geophys. Res.*, **116**, D07104, doi:10.1029/2010JD015127.

Son, S.W., N. F. Tandon, L. M. Polvani, and D. W. Waugh, 2009: Ozone hole and Southern Hemisphere climate change. *Geophys. Res. Lett.*, **36**, doi:10.1029/2009GL038671.

Spiegel,M.R., and Stephens, L. J. (1998), Statistics, edited by Barbara Gilson, Mcgraw-Hill, New York

Tebaldi, C., R. L. Smith, D. Nychka, and L. O. Mearns, 2005: Quantifying Uncertainty in Projections of Regional Climate Change : A Bayesian Approach to the Analysis of Multimodel Ensembles. *J. Clim.*, **18**, 1524–1541.

Tebaldi, C., and R. Knutti, 2007: The use of the multi-model ensemble in probabilistic climate projections. *Philos. Trans. A. Math. Phys. Eng. Sci.*, **365**, 2053–2075, doi:10.1098/rsta.2007.2076.

Thompson, D. W. J., J. M. Wallace, P. D. Jones, and J. J. Kennedy, 2009: Identifying Signatures of Natural Climate Variability in Time Series of Global-Mean Surface Temperature: Methodology and Insights. *J. Clim.*, **22**, 6120–6141, doi:10.1175/2009JCLI3089.1.

Thompson, D. W. J., and J. M. Wallace, 2000: Annular Modes in the Extratropical Circulation Part I : Month-to-Month Variability *. *J. Clim.*, **13**, 1000–1016.

Thompson, David W. J., J. M. Wallace, and C. H. Gabriele, 2000: Annular Modes in the Extratropical Circulation Part II : Trends *. *J. Clim.*, **13**, 1018–1036.

Vecchi, G. a., and B. J. Soden, 2007: Global Warming and the Weakening of the Tropical Circulation. *J. Clim.*, **20**, 4316–4340, doi:10.1175/JCLI4258.1. http://journals.ametsoc.org/doi/abs/10.1175/JCLI4258.1

Wallace, J. M., Y. Zhang, and L. Bajuk, 1996: Interpretation of Interdecadal Trends in Northern Hemisphere Surface Air Temperature. *J. Clim.*, **9**, 249–259,doi:10.1175/15200442(1996)009<0249:IOITIN>2.0.CO;2. doi:10.1175/JCLI-D-11-00166.1.

Wentz, F. J., L. Ricciardulli, K. Hilburn, and C. Mears, 2007: How much more rain will global warming bring? *Science*, **317**, 233–235, doi:10.1126/science.1140746.

Woollings, T., and M. Blackburn, 2012: The North Atlantic Jet Stream under Climate Change and Its Relation to the NAO and EA Patterns. *J. Clim.*, **25**, 886–902, doi:10.1175/JCLI-D-11-00087.1.